2017-01-01

An In-Depth Evaluation Of Shear Box Compactor For Hot Mix Asphalt

Isaac Jaime Aguilar
University of Texas at El Paso, ijaguilar2@miners.utep.edu

AN IN-DEPTH EVALUATION OF SHEAR BOX COMPACTOR FOR HOT MIX ASPHALT

ISAAC JAIME AGUILAR

Master's Program in Civil Engineering

APPROVED:

Imad Abdallah, Ph.D., Chair

Soheil Nazarian, Ph.D.

Chintalapalle Ramana, Ph.D.

Charles Ambler, Ph.D.
Dean of the Graduate School

Dedication

I would like to dedicate this thesis to my parents whose determination, diligence, and sacrifice has inspired me to continue my education.

AN IN-DEPTH EVALUATION OF SHEAR BOX COMPACTOR FOR HOT MIX ASPHALT

by

ISAAC JAIME AGUILAR, EIT, BSCE

THESIS

Presented to the Faculty of the Graduate School of

The University of Texas at El Paso

in Partial Fulfillment

of the Requirements

for the Degree of

MASTER OF SCIENCE

Department of Civil Engineering

THE UNIVERSITY OF TEXAS AT EL PASO

May 2017

Acknowledgements

I would like to thank my thesis advisor, Dr. Soheil Nazarian, for his guidance and support throughout my graduate career. I would like to also thank Dr. Imad Abdallah for providing me the opportunity to work at the Center for Transportation Infrastructure Systems (CTIS) and for offering his help and supervision even when things did not go as planned. I would also like to express my sincere gratitude to the CTIS laboratory manager, Mr. Jose Garibay, for providing me with sound advice and assistance in the laboratory. It has been an honor to work under all of them, and they have proven instrumental for this thesis. I am especially grateful for all the help I received from all the CTIS team, from the student volunteers to the staff, every step of the way.

To Dr. Ramana Chintalapalle, I would also like to express my gratitude for being my committee member and for taking the time to review this thesis. I would also like to express my sincere appreciation to one of my mentors while at UTEP, Ariana Arciero-Pino, who was the person who enabled me to perform my studies here. I would like to thank my fellow CTIS colleagues, Jorge Beltran and Victor Garcia for their help to make this thesis possible. I also want to thank my friends Diana Cabrera, Braulio Reyes, Juan Francisco Gonzales, Alejandra Escajeda, Eduardo Esparza and Rafael Lemus for their unconditional support and advice during those times I needed them most.

Finally, I would like to thank and dedicate this thesis to my family: my father, Jaime Aguilar De La Sancha, my mother, Edith Aguilar Martinez, and my sister, Erendy Vazquez Aguilar for always supporting and encouraging me, and for motivating me to persevere against the odds.

Abstract

Asphalt pavement is present in each roadway in every town or city today and it is paramount to properly design pavement to efficiently reduce its deterioration. To determine how pavement fails, pavement specimens prepared in the laboratory undergo performance tests which demonstrate the pavements strength and durability. Performance tests require little variability from compacted specimens, and it is critical to have a compaction method which is similar to field compaction and produces homogenous specimens. Currently, laboratory performance test specimens are obtained with the Superpave Gyratory Compactor (SGC). That device has few similarities to the rolling compactor, which performs the actual compaction of pavement in the field. To obtain precise and accurate performance test results, a compactor has to have an efficient compaction method and be able to produce repeatable test specimens. The PReSBOX Shear Box Compactor (SBC) was developed to simulate field compaction, since many test specimens can be extracted from the same sample, the specimens and as a result the performance test results can be more uniform.

The focus of this study was to determine whether SBC can produce compacted samples that were equal or improved as compared to SGC.

The distribution of air voids within compacted SBC samples and the comparison of performance tests which will be conducted using both the SBC and SGC were thoroughly studied herein. New specifications were developed for those to transportation agencies that would like to use SBC as an alternative to SGC.

Table of Contents

Acknowledgements iv

Abstract v

Table of Contents vi

List of Tables viii

List of Figures ix

Chapter 1: Introduction 1

1.1 Problem Statement 1

1.2 Organization of Thesis 2

Chapter 2: Literature Review 4

2.1 Background 4

2.1.1 Brief Overview of Compaction Methods 5

2.2 Shear Box Compactor 7

Chapter 3: Research Methodology 9

3.1 Study and Materials 9

3.2 Laboratory Test Methods 10

3.2.1 Overlay Tester (OT) 10

3.2.2 Indirect Tensile Test 16

3.2.3 Hamburg Wheel Tracking Device 17

3.3 Sample Preparation 19

Chapter 4: Results and Analysis 25

4.1 Air Void Distribution 25

4.2 Overlay Tester Results 30

4.3 Indirect Tensile Test Results 33

4.4 HWTD Results 35

4.5 Variability of Performance Tests 37

4.6 Compatibility of Results with SGC 40

Chapter 5: Summary, Conclusion, and Recommendations 43

5.1 Summary 43

5.2 Conclusions....43
5.3 Recommendations....43
References....45
Appendix A: Results with the SBC....47
Appendix B: Results with the SGC....59
Vita....75

List of Tables

Table 3.1: Information of the Different HMA Mixes 9
Table 3.2: Gradation Chart for the Different Mixes 10
Table 4.1: Air Void Properties of Sliced Samples for Type C Mix 26
Table 4.2: Sample and Specimen Information 29
Table 4.3: Summary of OT Results for SMA-D Mix 32
Table 4.4: Summary of OT Properties for all Mixes 33
Table 4.5: Summary of IDT Results for SMA-D Mix 34
Table 4.6: Summary of IDT Properties for all Mixes 35
Table 4.7: Summary of HWTD Results for SMA-D Mix 36
Table 4.8: Summary of HWTD Properties for all Mixes 37
Table A1: Summary of OT Results for Type-C Mix 48
Table A2: Summary of OT Results for Type-D Mix 50
Table A3: Summary of OT Results for TOM Mix 52
Table A4: Summary of IDT Results for Type-C Mix 53
Table A5: Summary of IDT Results for Type-D Mix 54
Table A6: Summary of IDT Results for TOM Mix 55
Table A7: Summary of HWTD Results for Type-C Mix 56
Table A8: Summary of HWTD Results for Type-D Mix 57
Table A9: Summary of HWTD Results for TOM Mix 58
Table B1: Summary of OT Results for Type-C Mix 60
Table B2: Summary of OT Results for Type-D Mix 62
Table B3: Summary of OT Results for SMA-D Mix 64
Table B4: Summary of OT Results for TOM Mix 66
Table B5: Summary of IDT Results for Type-C Mix 67
Table B6: Summary of IDT Results for Type-D Mix 68
Table B7: Summary of IDT Results for SMA-D Mix 69
Table B8: Summary of IDT Results for TOM Mix 70
Table B9: Summary of HWTD Results for Type-C Mix 71
Table B10: Summary of HWTD Results for Type-D Mix 72
Table B11: Summary of HWTD Results for SMA-D Mix 73
Table B12: Summary of HWTD Results for TOM Mix 74

List of Figures

Figure 2.1: Fatigue cracking and rutting pavement failures 4
Figure 3.1: OT Specimen during Testing Procedure 11
Figure 3.2: Typical OT Data 12
Figure 3.3: Interpretation of OT Results: a) Typical First Cycle Hysteresis Loop, b) Typical Second Cycle Hysteresis Loop, and c) Load Reduction Curve 13
Figure 3.4: a) Portion of Hysteresis Loop to Calculate b) Graphical Representation of Crack Propagation Rate c) Design Interaction Plot 15
Figure 3.5: IDT Machine Setup 16
Figure 3.6: HWTD Machine Setup 18
Figure 3.7: Illustration of SBC block production process: feeding (top left), laying (top right), compaction (bottom left), and finished product (bottom right) 20
Figure 3.8: Illustration of Compaction Sample Process with the SBC (IPC Global) 21
Figure 3.9: Loading Curves during the Compaction Process 23
Figure 3.10: Extraction of specimens for each performance test from a SBC sample 24
Figure 4.1: Sliced Compacted Sample from SBC 25
Figure 4.2: Sliced Samples Air Void Distribution for Type C Mix 26
Figure 4.3: Extraction of specimens for each performance test from a SBC sample 27
Figure 4.4: Distributions of Air Void Contents along Samples 1 and 2 27
Figure 4.5: Distribution of the Air Voids along back and bottom of Samples 1 and 2 28
Figure 4.6: OT Extraction Method 30
Figure 4.7: Overlay Tester Results for SMA-D Mix 31
Figure 4.8: Performance of SMA-D on Design Interaction Plot 32
Figure 4.9: IDT extraction method 33
Figure 4.10: IDT Load-displacement Response Curves for SMA-D Mix 34
Figure 4.11: HWTD Extraction Method 36
Figure 4.12: Rut Depth of Three Samples for SMA-D Mix 36
Figure 4.13: Average Overlay Tester Results for HMA Mixes 38
Figure 4.14: IDT Average Tensile Strength Performance Mixes Comparison 39
Figure 4.15: IDT Average Tensile Strength Performance Mixes Comparison 39
Figure 4.16: Average Air Voids for all Specimens 40
Figure 4.17: Design Interaction Plot Comparison of Mixes Performance 41
Figure 4.18: IDT Average Tensile Strength Performance Mixes Comparison 41
Figure 4.19: IDT Average Rutting Depth at 20,000 passes 42
Figure 5.1: Extraction of Other Types of Performance Tests 44
Figure A1: Results for Type-C Mix: a) First Cycle Hysteresis Loop, b) Second Cycle Hysteresis Loop, and c) Normalized Load Reduction Curves 47
Figure A2: Performance of Type-C on Design Interaction Plot 48
Figure A3: Results for Type-D Mix: a) First Cycle Hysteresis Loop, b) Second Cycle Hysteresis Loop, and c) Normalized Load Reduction Curves 49
Figure A4: Performance of Type-D on Design Interaction Plot 50
Figure A5: Results for Type-D Mix: a) First Cycle Hysteresis Loop, b) Second Cycle Hysteresis Loop, and c) Normalized Load Reduction Curves 51
Figure A6: Performance of TOM on Design Interaction Plot 52
Figure A7: IDT Load-displacement Response Curves for Type-C Mix 53

Figure A8: IDT Load-displacement Response Curves for Type-D Mix 54
Figure A9: IDT Load-displacement Response Curves for TOM Mix 55
Figure A10: Rut Depth of Three Samples for Type-C Mix 56
Figure A11: Rut Depth of Three Samples for Type-D Mix 57
Figure A12: Rut Depth of Three Samples for TOM Mix 58
Figure B1: Results for Type-C Mix: a) First Cycle Hysteresis Loop, b) Second Cycle Hysteresis Loop, and c) Normalized Load Reduction 59
Figure B2: Performance of Type-C on Design Interaction Plot 60
Figure B3: Results for Type-D Mix: a) First Cycle Hysteresis Loop, b) Second Cycle Hysteresis Loop, and c) Normalized Load Reduction 61
Figure B4: Performance of Type-D on Design Interaction Plot 62
Figure B5: Results for SMA-D Mix: a) First Cycle Hysteresis Loop, b) Second Cycle Hysteresis Loop, and c) Normalized Load Reduction 63
Figure B6: Performance of SMA-D on Design Interaction Plot 64
Figure B7: Results for TOM Mix: a) First Cycle Hysteresis Loop, b) Second Cycle Hysteresis Loop, and c) Normalized Load Reduction 65
Figure B8: Performance of TOM on Design Interaction Plot 66
Figure B9: IDT Load-displacement Response Curves for Type-C Mix 67
Figure B10: IDT Load-displacement Response Curves for Type-D Mix 68
Figure B11: IDT Load-displacement Response Curves for SMA-D Mix 69
Figure B12: IDT Load-displacement Response Curves for TOM Mix 70
Figure B13: Rut Depth of One Sample for Type-C Mix 71
Figure B14: Rut Depth of One Sample for Type-D Mix 72
Figure B15: Rut Depth of One Sample for SMA-D Mix 73
Figure B16: Rut Depth of One Sample for TOM Mix 74

Chapter 1: Introduction

1.1 Problem Statement

In mix design, a clear objective is set: to mix, compact, and test the asphalt mixture to determine its expected performance in service. The laboratory specimens prepared and tested during mix design should be ideally representative of field-compacted specimens. Hot mix asphalt (HMA) compaction in the field is performed by a rolling wheel compactor which compresses the asphalt with multiple passes over the surface. This compaction is achieved with large vibrational drums and the weight of the compacting vehicle. Contrary to field compaction, gyratory compaction methods are used to fabricate specimens for performance testing. The type of compaction method affects the physical properties of the specimens, such as aggregate particle orientation and void structure, because they depend on the method of compaction used (*Lu et al*. 2011). To obtain specimens which are true indicators of field performance, a compaction method that closely replicates field compaction and produces homogenous specimens is needed. In recent years, the use of gyratory compactors has become common, primarily because of the introduction of the Superior Performing Asphalt Pavements (Superpave) Mix Design Method. The Superpave Gyratory Compactor's (SGC) appeal is that it is a combination of a kneading compactor and a shear testing machine. The problem with gyratory compactors is that they only produce cylindrical specimens and there can be a large variability in the density of specimens (*Khan et al*., 1998). Therefore a new compaction device is necessary to produce test specimens with a limited variability and a closer similarity to field compaction.

The shear box compactor (SBC) was recently developed to compact large blocks of HMA mixtures where many specimens can be extracted from a single compacted sample. The specimens extracted from one sample can be a variety of shapes: beams, cylindrical or disk-shaped. The SBC

attempts to simulate field compaction by compacting the HMA mixture with a constant vertical force and a cyclic shear force with a constant maximum shear angle.

The objective of this thesis is to evaluate the performance of the SBC. Specimens compacted by the SBC were evaluated against specimens compacted by SGC. The following four types of asphalt mixtures were compacted on both devices: two traditional fine mixtures (coarse-grained Type-C and fine-grained Type-D as per Texas Department of Transportation, TxDOT), a fine-grained stone matrix asphalt (SMA-D), and thin overlay mixture (TOM). The following three types of performance tests were used to evaluate both devices: Overlay Tester (OT), Indirect Tensile Test (IDT), and the Hamburg Wheel Tracking Device (HWTD).

1.2 Organization of Thesis

Chapter 1 describes the problem statement of laboratory compaction and the objective of the study with the shear box compactor. Chapter 2 gives a brief review of past and current compaction methods and the standard compactors used in the industry today. Fatigue cracking and rutting, two types of roadway failures in pavement focused on in this study, are described.

Chapter 3 provides an overview of the research methodology carried out in this study. The properties of the different types asphalt material used are listed. Background on the performance tests used to evaluate the SBC as well as how to interpret the data are provided. The process of preparing a SBC sample and the air void study performed before performance testing are also shown. The compaction process of the SBC is described and displays of compacted samples in 3D that show the air void distributions in the samples are presented. The specimen extraction method for each performance test from a compacted sample is also displayed, as well as the compaction properties of all the specimens.

Chapter 4 summarizes all the results obtained from performance tests carried out on SBC specimens. The method used to prepare Overlay Tester (OT) specimens and the OT results are discussed. The method used to obtain Indirect Tensile Test (IDT) specimens from a compacted sample and the results are discussed. The method used to extract Hamburg Wheel Tracking Device (HWTD) specimens from a compacted sample and the results are also discussed. A final comparison and analysis of the performance test results is given to evaluate the SBC against the SGC.

Chapter 5 includes the conclusion and recommendations for future implementation of the SBC.

Appendix A contains the results of the performance tests on the SBC specimens, while Appendix B contains comparable results on the SGC specimens.

Chapter 2: Literature Review

2.1 Background

There are generally several layers in a flexible pavement that work together to distribute the vehicular loads over a larger area. These layers include the surface (HMA) layer, base, optional sub-base, and the subgrade. Each of these is made up of different types of materials which contribute to the structural support and drainage of the roadway. All layers are compacted by roller compactors to obtain higher densities, higher stability, and wear resistance. Over its design life, the roadway will deteriorate and will require maintenance and rehabilitation. Two common types of road failures are fatigue cracking and rutting seen in Figure 2.1.

Figure 2.1: Fatigue cracking and rutting pavement failures

Fatigue cracking is interconnected cracks on the surface course which are caused by repeated application of heavy wheel loads or lack of compaction strength from the base or subgrade. Rutting refers to the surface depressions in the wheel-path which occurs when there is compaction or mix design issues in the pavement and repeated application of load along the same wheel-path. To resist these failures, it is important and more cost efficient to evaluate the stability and performance of the HMA in the laboratory before it is placed in the field. Performance tests

in the laboratory can evaluate the fatigue cracking and rutting potential of HMA. By simulating field compaction and testing specimens in the laboratory, roadways can be efficiently designed. However, there is a major difference in laboratory compaction and field compaction. The three basic types of laboratory compaction methods, (impact compaction, kneading compaction, and gyratory compaction), do not use the roller compaction method as performed in the field. Shear box compactor was developed to simulate the roller compaction.

2.1.1 Brief Overview of Compaction Methods

The oldest type of laboratory compaction, the Marshall compaction, uses a mechanical hammer to prepare specimens by impact. This method was the primary mix design process used by state agencies for nearly 50 years. It provided a method for asphalt mix design by selecting the asphalt binder content at a density which would satisfy the minimum range of flow values and stability (*Swiertz et al.* 2010). The Hveem design method was introduced in the 1930's, where the specimens were fabricated using a kneading compaction by the California kneading compactor. The compactor applied a uniform series of moving impressions by a ram with a tamper foot onto the free face of the specimen. The entire surface area of the specimen was not covered while compacting, so as to produce a kneading action between the particles as the specimen rotated and compacted with each added blow. Gyratory compactors were developed in the 1930's by the TxDOT to simulate the increasing traffic pressures of vehicles operating on flexible pavements. In that compaction process, a vertical load and a self-adjusting kneading action were applied simultaneously (*McRae*, 1965).

An evolution of the gyratory compactor was produced when the Superpave Gyratory Compactor (SGC) was developed by the Strategic Highway Research Program (SHRP) (*Harman et al*., 2002). The SHRP researchers sought a device which would compact HMA specimens to the

densities attained under actual pavement climate and traffic conditions. That device is able to produce specimens for volumetric analysis, accommodate large aggregates, measure the specimen height, and provide data to indicate the density throughout the compaction procedure. The SHRP researchers then developed the SGC from a modified Texas Gyratory Compactor and other properties of previous compaction methods which produced cylindrical HMA specimens. In the compaction process, an HMA mixture is placed in a mold and then loaded onto the compaction apparatus where the SGC applies the required vertical pressure and angle of gyration to begin compaction (*Swiertz et al.* 2010).

While the SGC has been considered the best available compactor in the industry today, it has a number of drawbacks which introduce can variability into the compaction process (*Gabrawy,* 2000). The SGC can only produce cylindrical samples of limited size, and samples are compacted individually and successively. This procedure can take an extended amount of time if multiple samples are required and these samples will not be subjected to the same compaction temperature.

The PReSBOX Shear Box Compactor (SBC) was developed by IPC Global and Pioneer Road Services to simulate the action of a field compaction-roller (*Gabrawy,* 2000). SBC produces samples rapidly, while providing information about the mix workability and strength of the aggregate structure. In the compaction process, samples are confined in a steel mold with moveable sides while a constant vertical axial load and an increasing cyclic force is applied from the horizontal sides with a constant maximum shear angle to exert both compression and shear forces to the mixture. The SBC compactor features a PC interface for the user where compaction parameters are inputted and provides a graphical display of the following data: specimen height, vertical stress, shear stress and air voids per cycle

The produced samples are prismatic in shape with the following dimensions: 17.7 in. (450 mm) in length, 5.9 in. (150 mm) in width, and 5.7 – 7.3 in. (145 mm – 185 mm) in height. The samples fabricated are large enough to extract a variety of specimens, from beams to cylinders, with different dimensions depending on which performance test the user selects. With one single sample an HMA mix can be evaluated for fatigue cracking, rutting, or low-temperature cracking.

2.2 Shear Box Compactor

Qui et al. (2009) evaluated SBC beams for use with four point bending tests and studied the variability of the air void content between the extracted beams from the blocks. Their findings suggested that the initial air voids and the air voids after vertical load initiation can be used to investigate the workability of asphalt mixtures. They also found that there was no influence of difference in position in void content from the extracted beams. They recommended further comparisons between different types of mixtures to provide more information for further application of the SBC.

Qui et al. (2012) evaluated various SBC specimens with different geometries and properties, different gradations, asphalt binder types, sample geometries, and sampling positions. They found that asphalt mixtures with larger aggregate sizes required a higher shear stress and more shear cycles to reach the target air voids content. The asphalt binder type had no influence on their compaction curves. The total variation of all the measured air voids of all the test specimens were about 2%, while within one asphalt block the variation of the measured air voids was less than 1% regardless of the mixture composition, binder type, and specimen shape. They also found that the specimens obtained from the upper part of the block were more compacted than the lower part of the block. A 1% higher air voids content was observed when the asphalt specimens were taken close to the side of the asphalt block compared to those taken from the middle of the block. In their finite element simulation assessment, the results indicated that the shear and compressive stresses are distributed homogeneously in the middle of the asphalt block.

No shear was observed at 20 mm from the block sides, and the upper part of the block had a slightly higher shear stress than the lower part.

Li (2013) investigated the effect of specimen size and test type on laboratory fatigue test results of HMA using the SBC for sample preparation. Li used cylindrical and rectangular specimens for the tests and trimmed of 20 mm from all specimens' edges to avoid inadequate compacted parts of the block. He was found that the upper part of the block had a higher density than the lower part, which agreed with the results reported by Qui (2012). The upper part of the block also experienced more shear stress than the lower part, which had an effect on the distribution of air voids also seen by Qui (2012).

Chapter 3: Research Methodology

3.1 Study and Materials

In this study, four different HMA mixes were compacted by the SBC and SGC: Traditional dense-graded mixtures (Type-C and Type-D as per TxDOT), stone-matrix asphalt (SMA-D), and thin overlay mix (TOM). The general purpose Type C and Type D mixes are used extensively throughout Texas since they are well-graded, relatively impermeable, and are cheaper than other mixes. SMA-D and TOM are the gap graded mixes that are generally more expensive due to being composed of a higher quality of aggregates and modified binder. They are known for their durability and rut resistance. Table 3.1 shows the general information for the different mixes, such as the type of asphalt binder it contains and how much asphalt content each mix contains. Table 3.2 shows the gradation for each mix. All mixes follow TxDOT standards.

Table 3.1: Information of the Different HMA Mixes

Mix Type	Location	Asphalt Binder	Asphalt Content, %	Binder Source	Mixing Temperature, °F
Traditional Fine Mixture (Type-C)	El Paso	PG-64-22	4.6	Jobe Materials	290
Traditional Fine Mixture (Type-D)	Brownwood	PG-64-22	5.1	Jebro	290
Stone-matrix Asphalt (SMA-D)	Lubbock	PG-70-28	6.3	NA	325
Thin Overlay Mix (TOM)	Austin	PG-76-22	6.5	Asphalt Inc	325

Table 3.2: Gradation Chart for the Different Mixes

Sieve	Type-C	Type-D	SMA-D	TOM
3/4"	99.3	100	100	100
1/2"	-	100	98.4	100
3/8"	82.4	98.5	71.3	98.9
No. 4	52.7	68	23.2	47.3
No. 8	36.9	37.5	20	21.8
No. 16	-	-	17.1	16.5
No. 30	18.6	15.5	16.3	12.9
No. 50	14	11	13.1	10.6
No. 200	5.6	3.4	10	6.3

3.2 Laboratory Test Methods

The following three different performance tests were used to evaluate the SBC and SGC.

3.2.1 Overlay Tester (OT)

The Overlay Tester (OT) is a fatigue testing machine designed in the 1970's to model displacements caused by thermal stresses in asphalt pavements resulting from cyclic changes in the surrounding temperature (Germann et al., 1979). The OT was developed to evaluate the reflective cracking resistance of asphalt overlays generated by vehicle loading and changes in temperature: the opening and closing of joints or cracks are the main driving forces inducing reflection crack initiation and propagation. The setup of the machine consists of two steel plates: one fixed while the other slides horizontally to simulate the opening and closing of joints or cracks in the pavements beneath an overlay (Zhou et al., 2003). With this simulation of vehicle loading, the OT measures the number of cycles to failure of HMA specimens. An OT specimen during testing is shown in Figure 3.3.

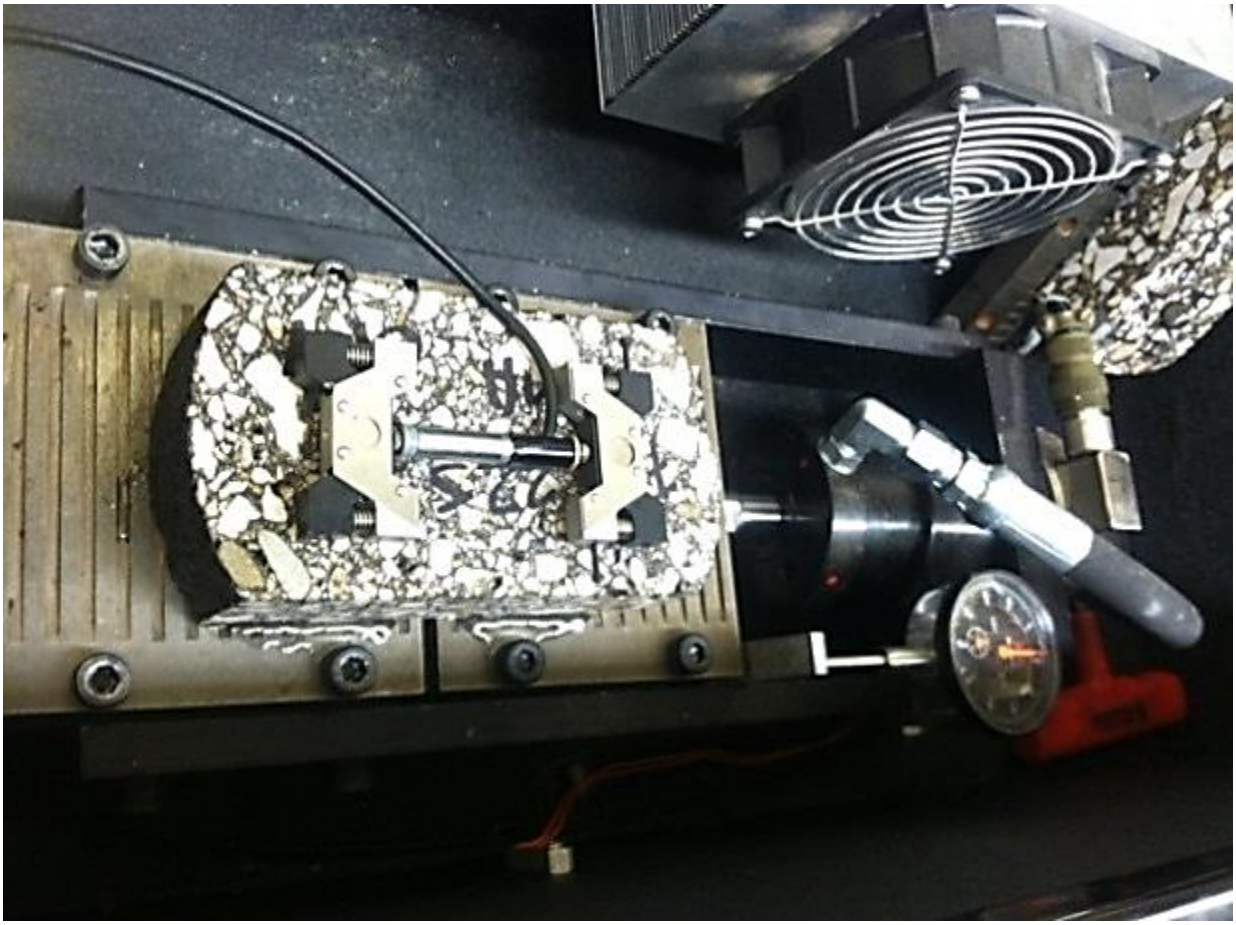

Figure 3.1: OT Specimen during Testing Procedure

The specification of the OT test procedure has been outlined in the TxDOT test procedure designation Tex-248-F. The OT test is an electro-hydraulic system that applies tensile displacements to the HMA specimens and is conducted in a displacement-controlled mode at a repeated loading rate of one cycle per 10 sec. The maximum separation of the steel plates reach is 0.025 in. (0.635 mm) at a test temperature of 77ºF (25ºC). A linear variable differential transformer (LVDT) can be placed on top of the specimen to measure the displacement, but it is not required by specifications. The OT test will display the number of cycles of applied load until the failure of the specimen. This failure is explained by Zhou et al (2006): it is the maximum load the specimen experiences at a given cycle 93% less than the maximum peak load from the first cycle.

From one compacted SBC sample, 9 OT specimens were extracted. The OT specimen's dimensions were: 6 in. (150 mm) long, 3 in. (75 mm) wide, and 1.5 in. (38 mm) thick. A compacted sample from the SBC would first be produced, and later another cylindrical sample would be cored from the SBC sample using a water-cooled core drill to obtain sample with a 6 in. (150 mm) diameter and 6 in. (150 mm) height. Then each cylindrical sample would then be cut and trimmed to produce three OT specimens. Figure 3.2 shows the typical data produced from the OT test which the device automatically records. From this recorded data the user can develop the hysteresis loops from the displacement and load acquired for each cycle.

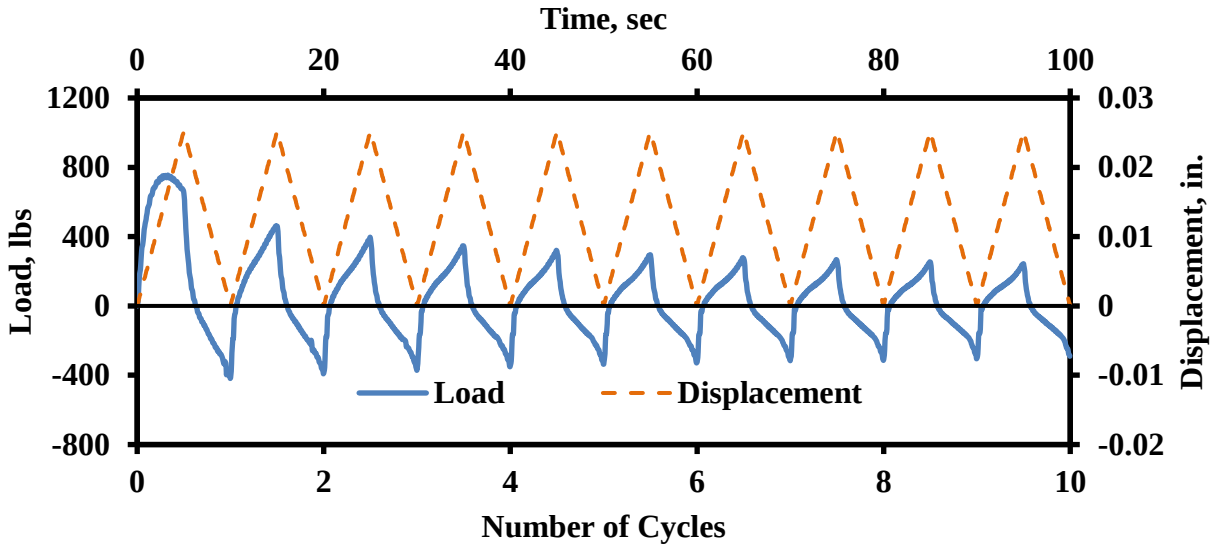

Figure 3.2: Typical OT Data

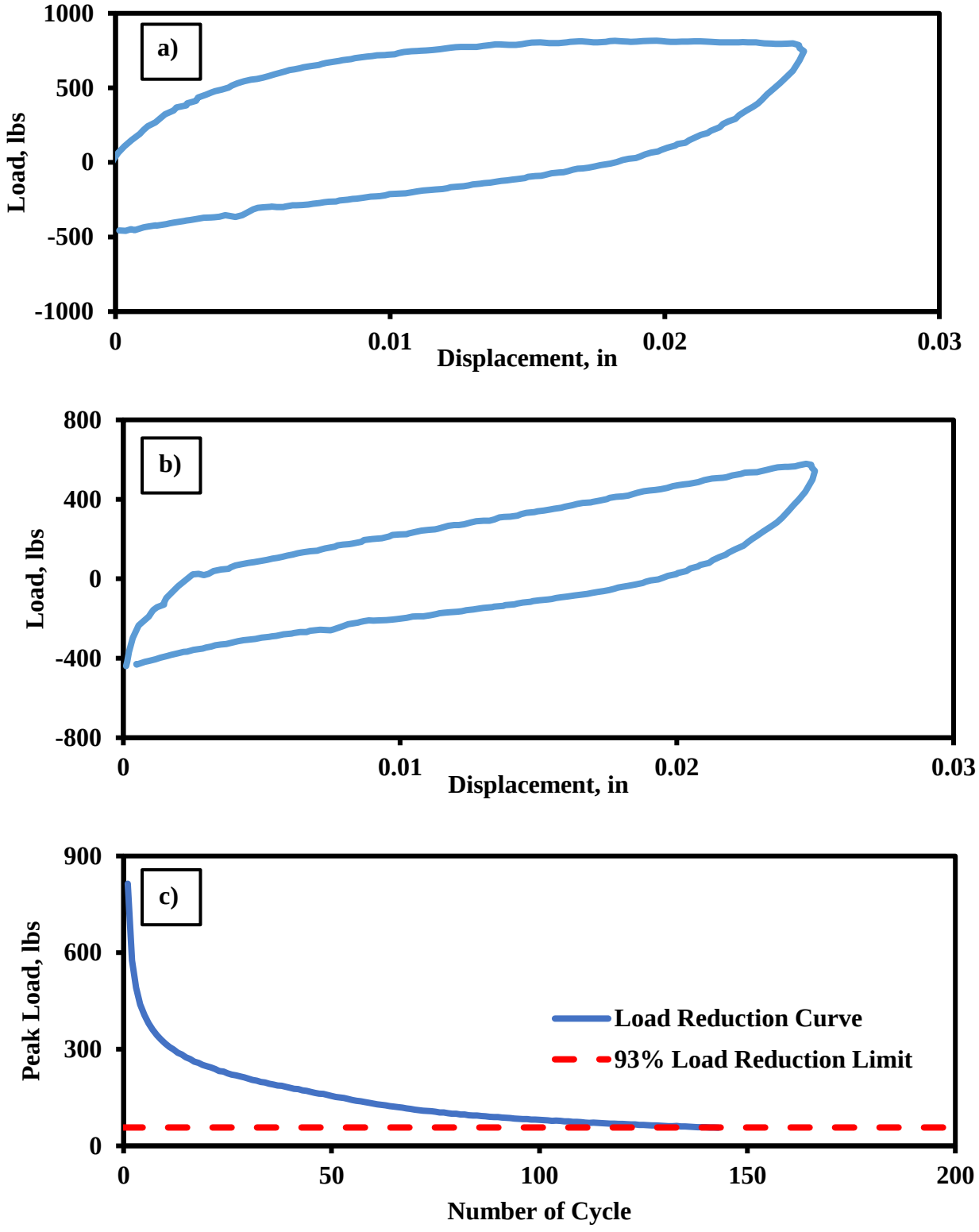

Figure 3.3: Interpretation of OT Results: a) Typical First Cycle Hysteresis Loop, b) Typical Second Cycle Hysteresis Loop, and c) Load Reduction Curve

The hysteresis loops can be plotted on one another to view the behavior of the HMA mixture as seen in Figure 3.3. The first cycle provides the maximum load where the initial crack occurs as seen in Figure 3.3a. After the first cycle, the remaining cycles display the crack propagation phase until the failure limit of 93% maximum load is reach as shown in Figure 3.3c.

While studies have considered the OT test as reliable (Bennert et al., 2008, Hajj et al., 2010), there has been variability in the reported repeatability results of the OT. Walubita et al. (2012) noted the cause of variability in the results occurred because of the following differences in the laboratory: specimen preparation and machine calibration. To further evaluate sources of variability, Garcia and Miramontes (2015) studied several potential sources such as the specimen preparation and testing mechanisms by evaluating key steps in the OT test procedure. They proposed a data interpretation method which involved two phases of the OT test: crack initiation and crack propagation. The number of cycles to failure parameter was used determine the fatigue life of HMA, but a high variation in test results required new parameters to be sought. Instead the critical fracture energy and crack progression rate was chosen in their study to properly evaluate HMA mixes. Critical fracture energy is the energy required for the AC mix to initiate the crack and the area is illustrated in Figure 3.4a. The crack progression rate shows how fast the crack propagates through the AC specimen and therefore also shows the fatigue life of that AC mixture. Figure 3.4b shows the variation of the crack driving forces against the number of cycles. The crack propagation was quantified by fitting a power equation to the load reduction curve to smooth uncertainties in the load measurements. The power coefficient of the equation is then interpreted as the crack progression rate. The design interaction plot was created in Figure 3.4c to evaluate the cracking resistance of AC mixtures. As an initial failure limit, a crack progression rate of 0.5 was determined if the mix was stiff or poor in cracking resistance.

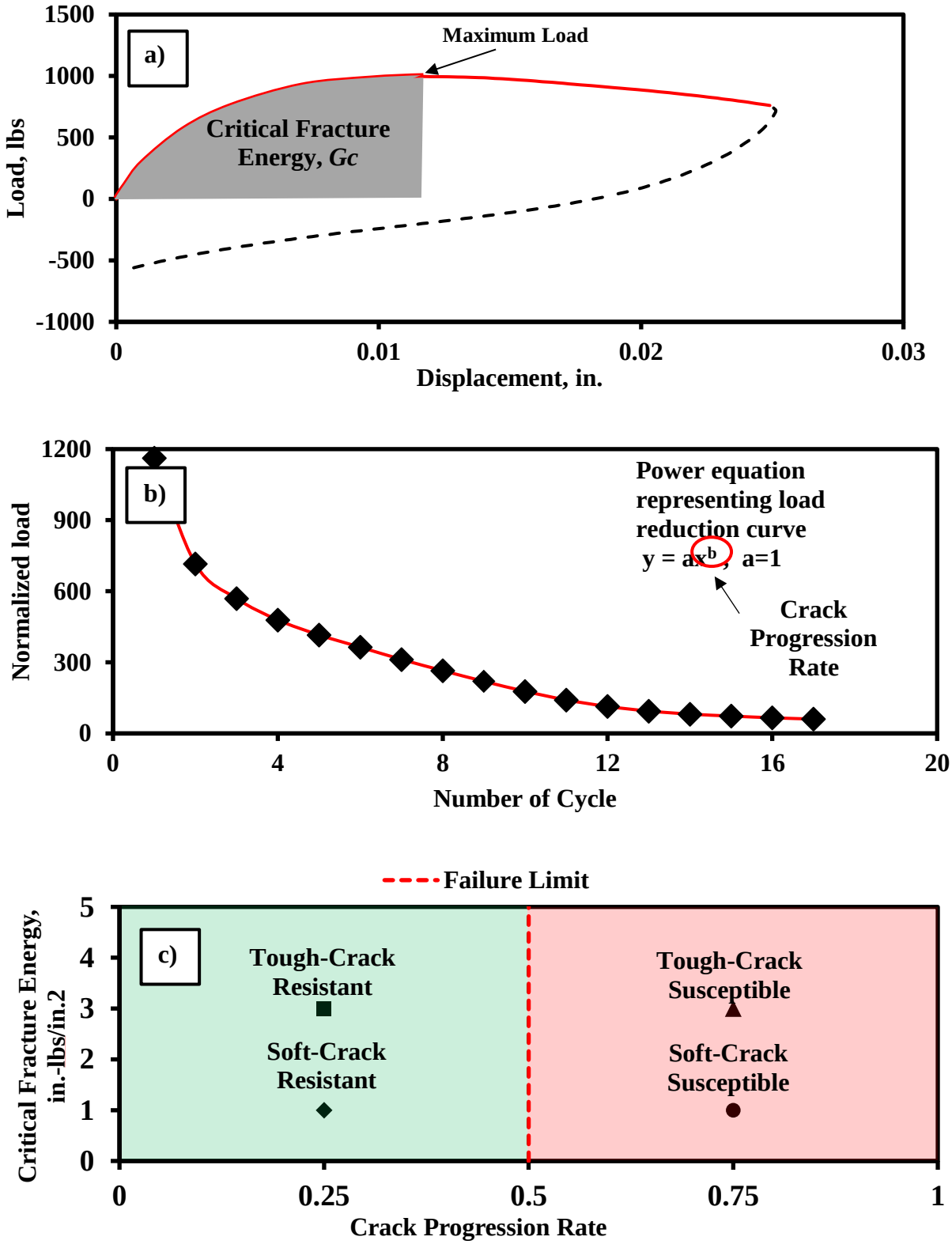

Figure 3.4: a) Portion of Hysteresis Loop to Calculate b) Graphical Representation of Crack Propagation Rate c) Design Interaction Plot

3.2.2 Indirect Tensile Test

The Indirect Tensile Test (IDT) test is used to estimate the tensile strength of mixes and is performed at a much faster loading rate than the OT. The IDT tests were performed following ASTM D693, "Test Method for Indirect Tensile (IDT) Strength of Bituminous Mixtures." The IDT has been used in structural design research for flexible pavements since the 1960s and in HMA mixture design research. It is a practical and effective test for determining the elastic tensile properties and distress related properties of HMA (Kennedy et al., 1983). The IDT is performed by loading a cylindrical specimen with a single or repeated compressive load, which acts parallel to and along the vertical diametral plane as seen in Figure 3.5.

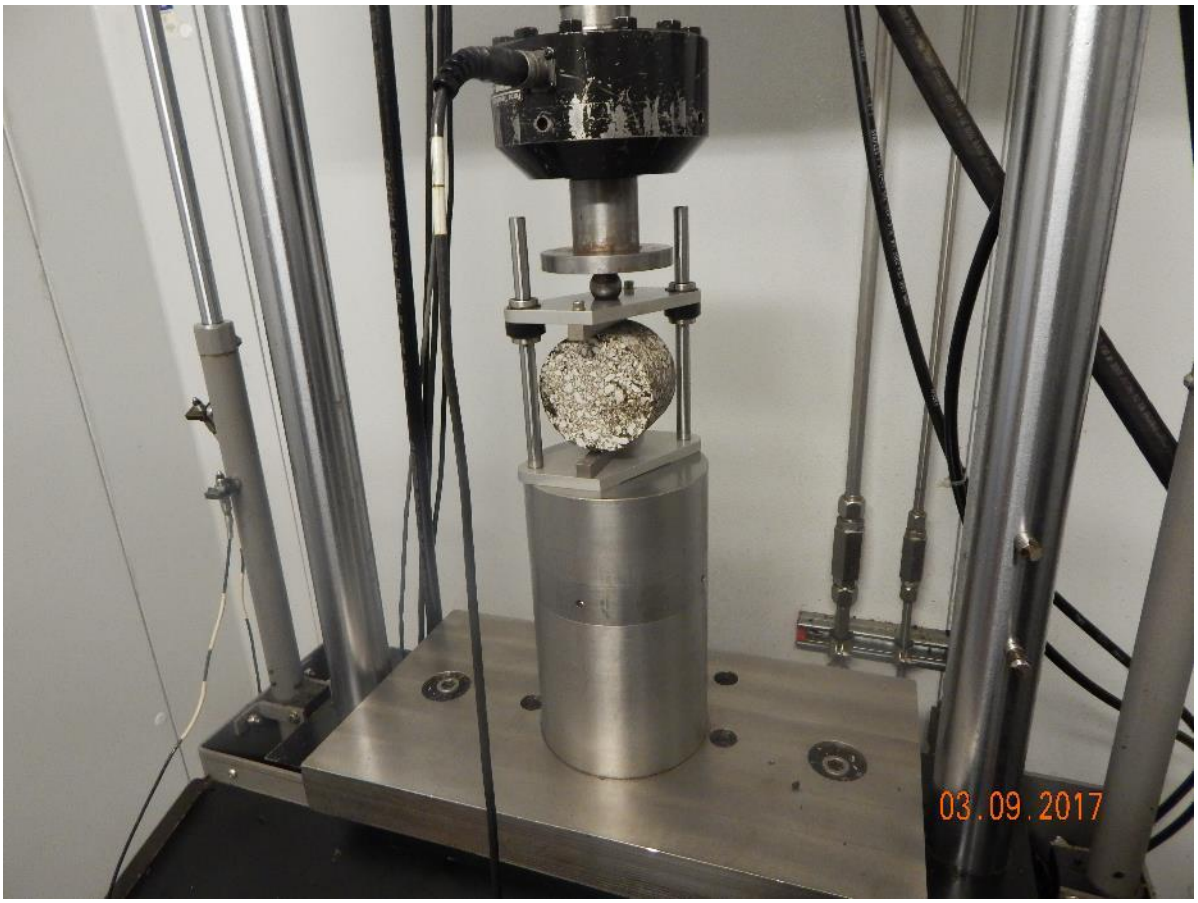

Figure 3.5: IDT Machine Setup

With this loading set up, relatively uniform tensile stress develops perpendicular to the direction of the applied load and along the vertical diametral plane, which causes the specimen to fail by splitting along the vertical diameter. The calculated failure at the peak load is the strength of a specimen and of the HMA mix. The current TxDOT asphalt content (AC) mix design specifications for the maximum and minimum limits for IDT are: a maximum allowable strength of 200 psi and a minimum allowable strength of 85 psi for dense graded mixes.

Six specimens were cored from one compacted sample for each mix. The dimensions for the specimens were 2.4 in. (61 mm) thick and a dimeter of 4 in (102 mm). The specimens were conditioned to a temperature of 77°F in an environmental chamber before the tests were performed for at least an hour and the tests were also conducted the chamber to ensure the temperature stayed constant during the test.

3.2.3 Hamburg Wheel Tracking Device

The Hamburg Wheel Tracking Device (HWTD) was developed in the 1970s in Hamburg, Germany (Romero and Stuart 1998). The HWTD measures the combined effects of rutting and moisture damage by rolling a steel wheel across the surface of an asphalt specimen immersed in hot water. In the testing procedure, both steel wheels roll back and forth on the submerged specimens until the wheels pass 20,000 times or until 12.5 mm of deformation is reached. Originally, a pair of cubical or beam test specimens were used, but cylindrical specimens compacted with the SGC are now used. In this study rectangular blocks were chosen as the specimens and new jigs were constructed to fit the specimens onto the device as shown in Figure 3.6. The specimens are arranged in a series to provide the required path length for the wheels and

the rut depth is measured continuously with a series of LVDT's on the sample.

Figure 3.6: HWTD Machine Setup

The results from the HWTD are as follows: the post compaction consolidation, creep slope, stripping slope and stripping inflection point. The post compaction consolidation is the rut depth measured at 1,000 passes, assuming that the wheel is densifying the mixture within the first 1,000 wheel passes. The creep slope is used to evaluate rutting potential and it is the number of wheel passes to produce a 1 mm rut depth due to viscous flow. The stripping slope is measured as the number of passes required to create a 1 mm impression from stripping and it is a measure of the accumulation of moisture damage. The stripping inflection point is the number of passes at the

intersection of the stripping slope and the creep slope. This point represents the moisture damage potential of the HMA and is the initiation of stripping (Aschenbrener and Currier 1993).

The HWTD specimens were obtained by cutting a sample into six different rectangular sections. Six specimens were then extracted from one compacted sample from each mix. The HWTD specimens' dimensions were the following: 2.4 in. (61 mm) thick, 5.9 in. (150 mm) in width and 5.6 in. (143 mm) in length. Three HWTD tests were then performed and each test lasted 20,000 passes. Wooden jigs were constructed to keep the specimens firmly in place while the tests occurred at a constant temperature.

3.3 Sample Preparation

The sample preparation process were performed according to ASTM D7981, "Standard Practice for Compaction of Prismatic Asphalt Specimens by Means of the Shear Box Compactor." The rectangular block produced by SBC has a fixed length and width of 17 in. (450 mm) x 5.9 in. (150 mm), while the height can range from 5.7 in. (145 mm) to 7.2 in. (185 mm). In this study a fixed height of 6 in. (152.4 mm) was chosen for all the compacted samples. The equipment required to compact a SBC sample consists of: three or four pans, a tamping rod, a grease remover, and a heating jig. It is essential to follow the instructions by IPC Global when turning on and turning off the SBC. If the SBC is inappropriately turned on or off, the SBC will have trouble connecting to the software and the SBC will lose its connection when compacting a sample.

The sample preparation is critical phase when compacting with SBC. It should be repeated in the same manner for each compaction so variability is not introduced in the process. Only one sample per day was compacted due to the difficulty in moving a finished sample off the SBC, which could lead to the breakage of the sample. In the beginning, a compacted sample would be produced by using only two trays of material and no preheating of the SBC machine. This method

was quick and efficient yet there would be differences in the target air void content for each compacted sample. The ASTM method was then followed, using a preheated jig and distributing the sample material into four trays which displayed more consistent results. Figure 3.7 highlights important steps of the compaction procedure for the SBC of an HMA sample. The compaction process is shown for one sample in Figure 3.8.

Figure 3.7: Illustration of SBC block production process: feeding (top left), laying (top right), compaction (bottom left), and finished product (bottom right)

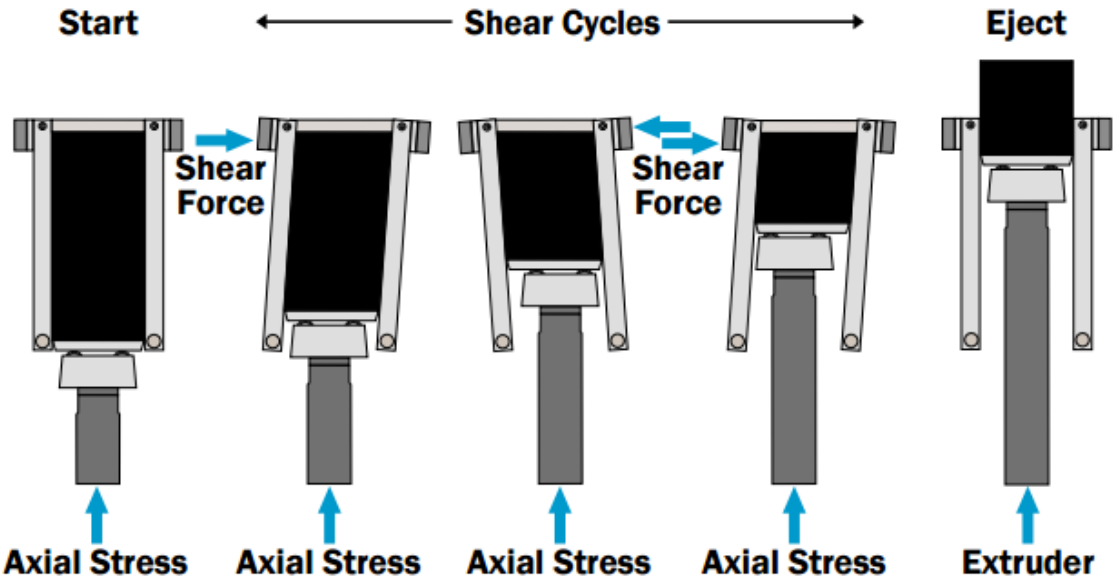

Figure 3.8: Illustration of Compaction Sample Process with the SBC (IPC Global)

The following steps are followed in order to prepare a specimen:

(1) Preheating: Before the compaction of an actual sample, it is recommended to pour and compact a hot sample into the mold to allow all the machine components to heat up. In this study, a steel box jig was developed and heated to the selected compaction temperature for at least 45 minutes before it was placed into the compaction mold instead of a hot sample. The mold plates and wearing plates were also placed in the oven at the selected compaction temperature for at least 45 minutes prior to loading the mix in the compactor. The mold plates and wearing plates were thoroughly cleaned with a grease remover to ensure a clean compacting surface.

(2) Mixing: The total mass of a HMA sample is typically 45 – 55 lb (25 – 30 kg) for one block and therefore it is recommended to evenly distribute this mass onto about 3 – 4 preheated trays to easily manage the material mass. These trays are then placed in the oven until the target compaction temperature is reached.

(3) Feeding: The preheated steel bottom plate and wear plate are placed at the bottom of the compaction mold, and then the preheated chute box is placed on top of the plates with the bottom gate closed. The feeding process starts when the HMA meets the selected compaction temperature. First two trays of the loose mixture are fed carefully into the chute, alternating the side of the chute into which the mixture is first poured in. The bottom gate of the chute box is then released to allow the mixture to fall into the compaction mold and the chute box was removed.

(4) Laying: A long tamping rod is used to poke the mix five times near each of the four vertical corners of the mold. The mixture is then properly distributed at all four corners within the mold to ensure the mixture is evenly spread. The preheated loading chute is placed back on top of the compaction mold, and the previous step, feeding, is repeated for the last two trays of mixture. The preheated steel top plate and wear plate are placed on top of the mix. The mold is then slid into the frame and locked to begin compaction.

(5) Compaction: Before the start of compaction, the following required input data are added to the computer: sample weight, vertical stress, shear angle, target height and the maximum density. There are four termination criterions for compaction with the SBC: cycles, height, density, and air voids.

(6) The compaction process is shown for one sample in Fig 3.8. Figure 3.8 displays the forces applied to the sample. A constant vertical force of 600 kPa is applied to provide the required vertical stress. A cyclic shear angle of 4º is applied to the sample. When the height termination criterion of 6 in. (152 mm) is met, the framework centers itself and the loading is released. The block is ejected by an air pump and allowed to cool down for one day.

(7) Sampling: After one day, the block is subjected to sampling as shown in Figure 3.10. The blocks are either sawn or cored into different sizes of beams or cylinders. The extraction of test specimens from an SBC sample were carried out into three sections: the front which faced away from the SBC, the middle, and the back which was the part closest to the SBC.

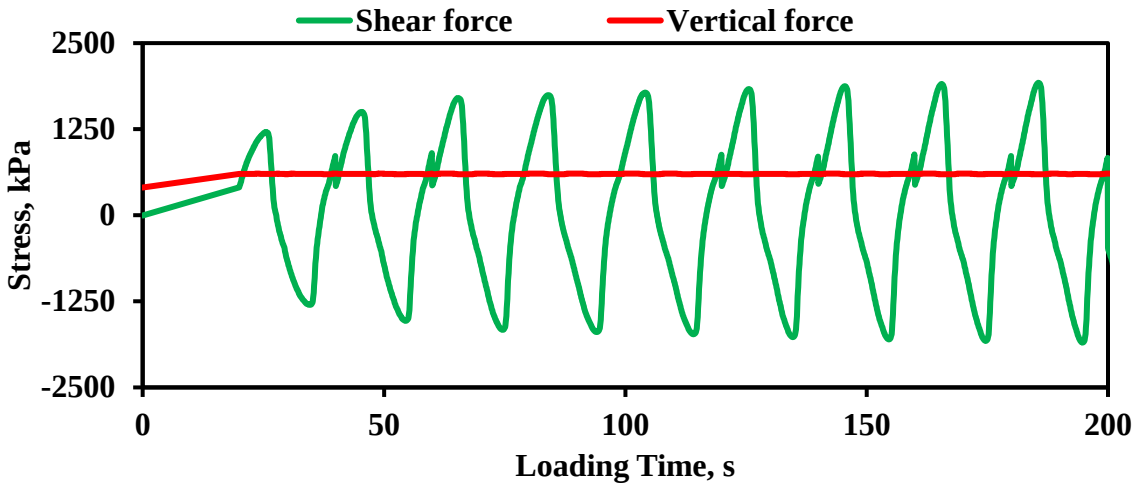

Figure 3.9: Loading Curves during the Compaction Process

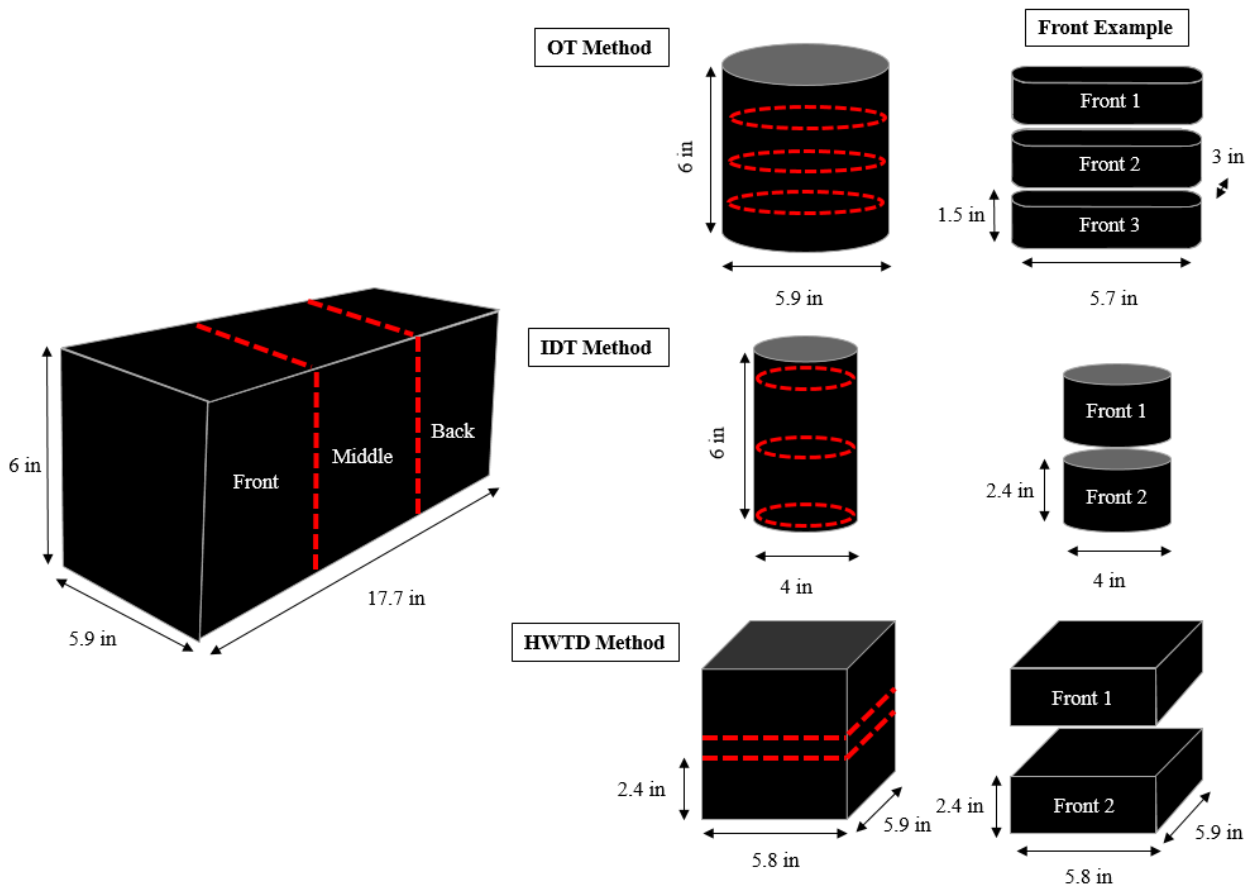

Figure 3.10: Extraction of specimens for each performance test from a SBC sample

A naming system was used to identify which section the specimen was extracted from. The sections were labeled front, middle, and back horizontally along the 17.7 in. (450 mm) length of the sample. From each section specimens were extracted and labeled one, two, and three vertically along the 6 in. (152 mm) length of the sample. Only the OT tests had a third level of specimens for each section.

Chapter 4: Results and Analysis

4.1 Air Void Distribution

The air void content that is inversely related to the density of a mixture affects the performance of the HMA mix. Usually air void contents between 3% and 8% produce the best compromise of pavement strength, fatigue life, and moisture susceptibility. In performance testing in the laboratory, an air void content of 7% ± 1% is set as the standard to achieve by many highway agencies.

Before the performance tests were conducted, the variations in the air void content were examined for the traditional fine mixture (Type-C). Two samples were compacted to a nominal air void content of 7% ± 1% and sliced as seen in Figure 4.1. The first slice corresponded to the front part of the sample which faced away from the SBC while the ninth slice corresponded to the back of the sample which was closest to the SBC.

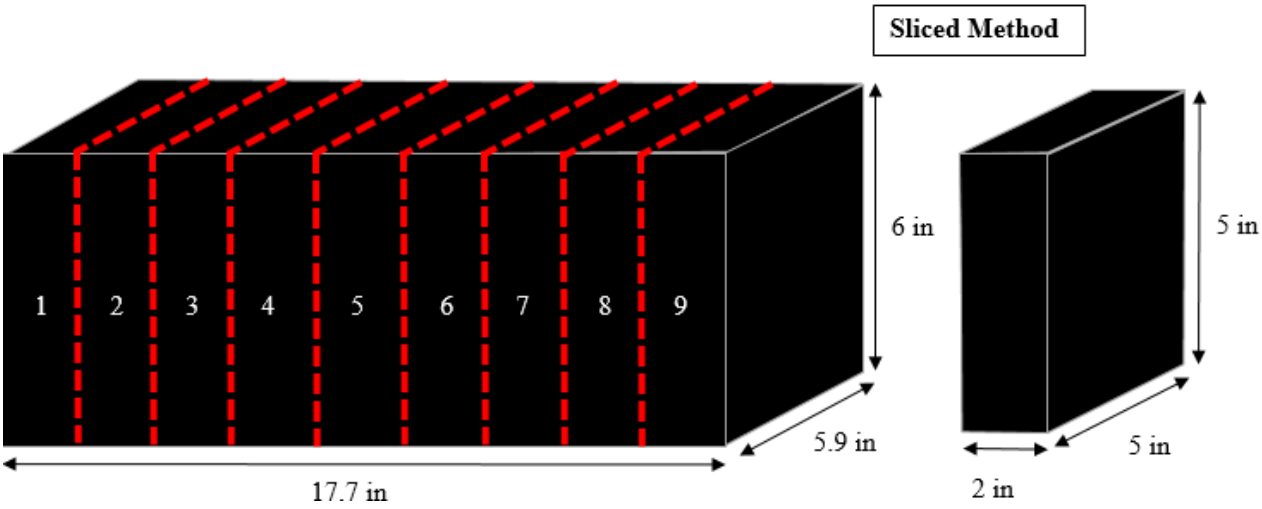

Figure 4.1: Sliced Compacted Sample from SBC

The variations in air void content of the nine slices for the two samples are shown in Figure 4.2. The air void contents of the two samples differed slightly as reflected on Table 4.1. Both

samples required the same number of compaction cycles to achieve their target density. For both samples, the average air void content was close to 7% with a COV of about 3%.

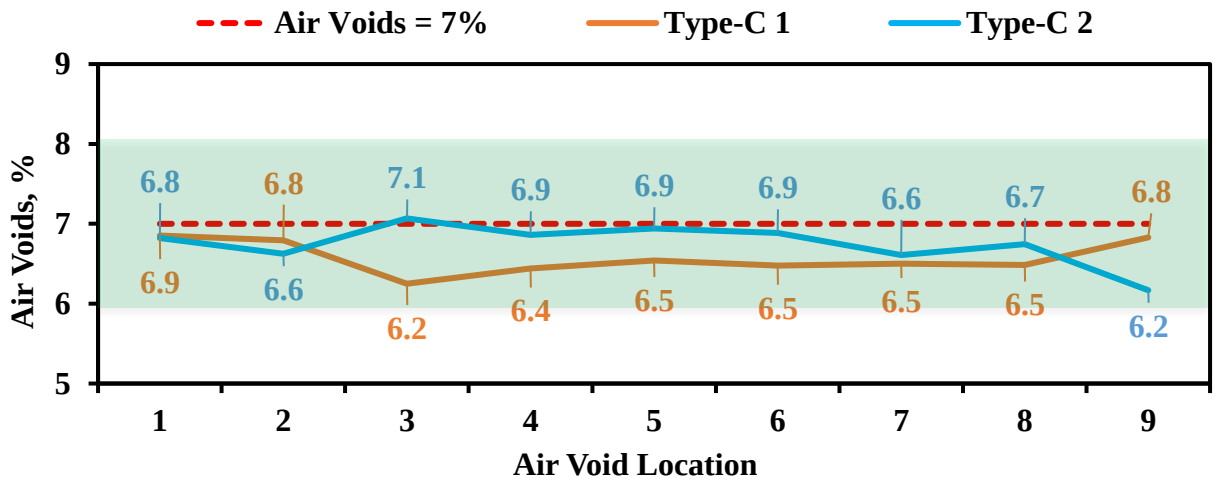

Figure 4.2: Sliced Samples Air Void Distribution for Type C Mix

Table 4.1: Air Void Properties of Sliced Samples for Type C Mix

Sample	Number of Cycles	Average Air Voids, %	Max. Air Voids, %	Min. Air Voids, %	Standard Deviation	COV, %
1	4	6.6	6.9	6.2	0.2	3.0
2	4	6.7	7.1	6.2	0.2	3.7

Each slice was then further split into nine cubes as shown in Figure 4.3. The distributions of the air void content from the 81 cubes for each of the two samples are shown side by side in Figure 4.4. Sample 1 is on the left side while Sample 2 is on the right in both Figures 4.4a and 4.4b. Sample 1 has a higher air void content near its surface than Sample 2.

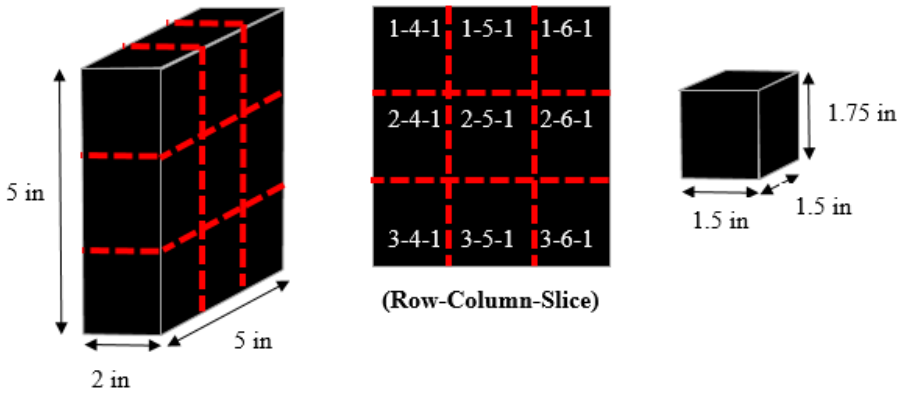

Figure 4.3: Extraction of specimens for each performance test from a SBC sample

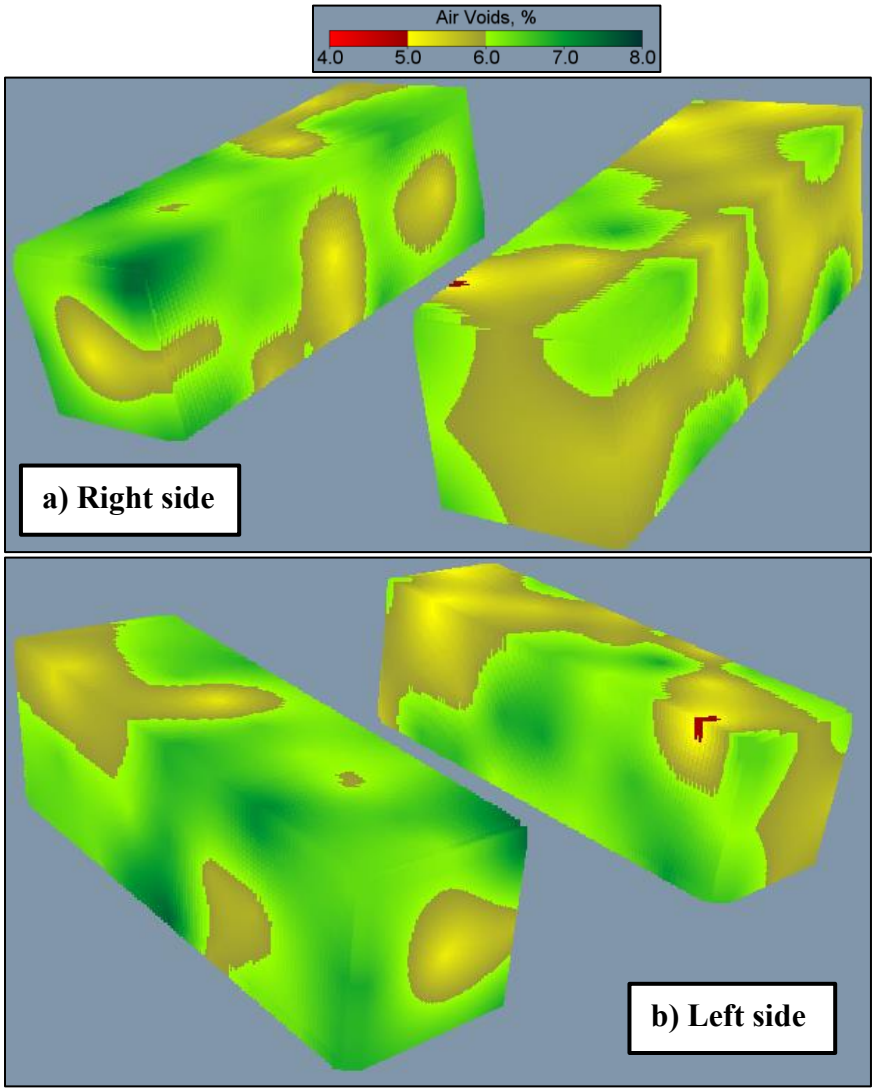

Figure 4.4: Distributions of Air Void Contents along Samples 1 and 2

The back and bottom views of the distribution of air void contents for both samples are shown in Figure 4.5 with Sample 1 being on the right and Sample 2 on the left. For both samples, the air void contents are similar with only patches of low air voids.

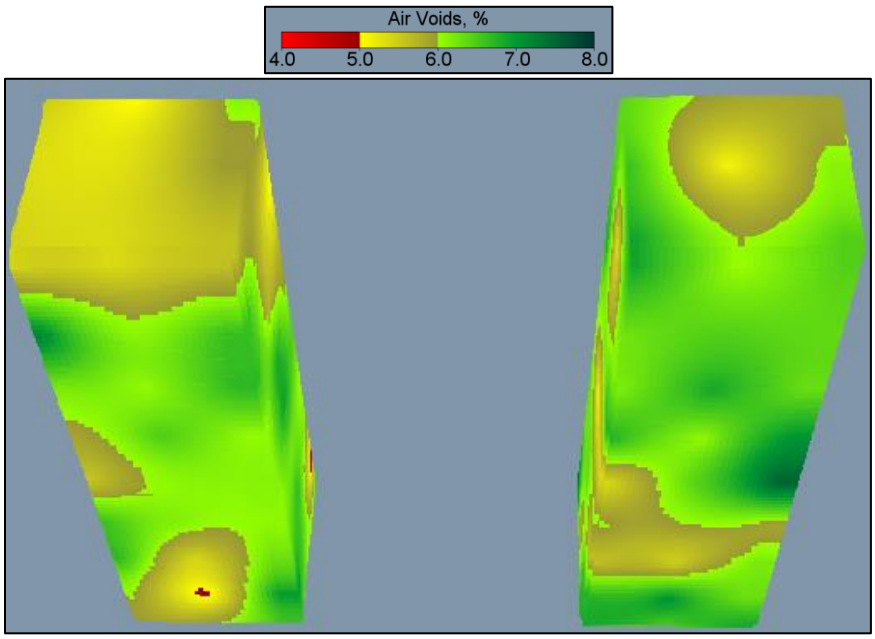

Figure 4.5: Distribution of the Air Voids along back and bottom of Samples 1 and 2

Table 4.2 contains an overview of the variations in the air void contents of all samples prepared for this study as presented in Appendix A. The COV's of the air void contents for the Type-C and Type-D samples were less than 10%, while the SMA-D and TOM samples exhibited air void content COV's of more than 10%. The least amount of time was needed to compact the Type-C samples. The Type-D and TOM samples required over ten cycles to reach the 7% ± 1% air void content for the OT and IDT tests. The HWTD samples for all mixes required almost double the number of cycles to reach the 7% ± 1% air void content. This occurred because non-standard specimen blocks were used (see Figure 3.10), instead of the standard cylinders as prescribed in test procedure Tex-242-F. The reason and process for this pattern are described below.

In the first trial, cylinders were cored from a compacted SBC sample. By removing the surface exterior, the cylindrical specimens were too small to fit into the HWTD testing molds. In the second trial, non-standard blocks were used. The non-standard blocks are rectangular prisms with the dimensions of 5.8 in. (147 mm) in length, 5.9 in. (150 mm) in width, and 2.4 in. (61 mm) in height. These specimens exhibited higher air void contents due to the blocks having more surface area. Therefore the second trial was also discarded. A third trial was conducted were more material was used in the compaction process to achieve the required 7% ± 1% air void content. The results for the third trial are shown in Table 4.2 and the procedure used in the third trial was used consequently in later mixes. Due to the added mass, the HWTD samples for all mixes required almost double the number of cycles to reach to 7% ± 1% air void content.

Table 4.2: Sample and Specimen Information

Mix	Test	Number of Cycles	Average Air Voids, %	Max. Air Voids, %	Min. Air Voids, %	Standard Deviation	COV, %
Type-C	OT	2	7.2	8.0	6.2	0.5	7.5
	IDT	2	7.7	8.3	7.0	0.5	6.2
	HWTD	4	7.5	7.7	7.2	0.2	2.1
Type-D	OT	14	7.8	8.9	6.4	0.8	9.6
	IDT	11	6.9	7.7	6.2	0.4	6.4
	HWTD	21	7.8	8.5	6.9	0.5	6.8
SMA-D	OT	6	7.1	8.7	5.7	0.9	13.3
	IDT	7	8.1	10.7	7.0	1.2	15.2
	HWTD	14	6.6	7.7	5.1	1.0	15.2
TOM	OT	15	7.5	9.5	6.0	1.1	14.0
	IDT	11	7.8	8.7	6.8	0.6	8.0
	HWTD	33	6.8	7.9	5.6	0.8	11.6

4.2 Overlay Tester Results

In this and subsequent sections, the test results from the SMA-D samples are presented as illustrative examples. The corresponding results for samples of all mixes prepared with SBC are shown in Appendix A and the SGC are shown in Appendix B.

Figure 4.6 displays how the nine specimens were extracted from one sample. The typical results, in terms of the maximum load achieved, displacement, and the number of cycles, for each specimen are shown in Figure 4.7. Most specimens extracted from one sample behaved similarly. Figure 4.8 presents the performance of each specimen in the OT design interaction plot. Most specimens are clustered closely.

Table 4.3 provides the salient properties of each specimen, such as the calculated critical fracture energy and the crack progression rate. All OT tests were terminated at cycle 200 as recommended by Garcia et al. (2017). With a COV of 13% for air void contents, the COV's of the extracted results varied between 9% and 21%.

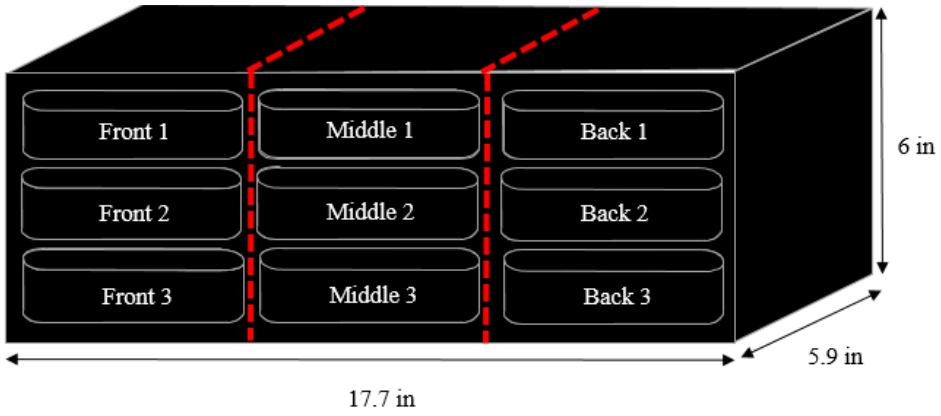

Figure 4.6: OT Extraction Method

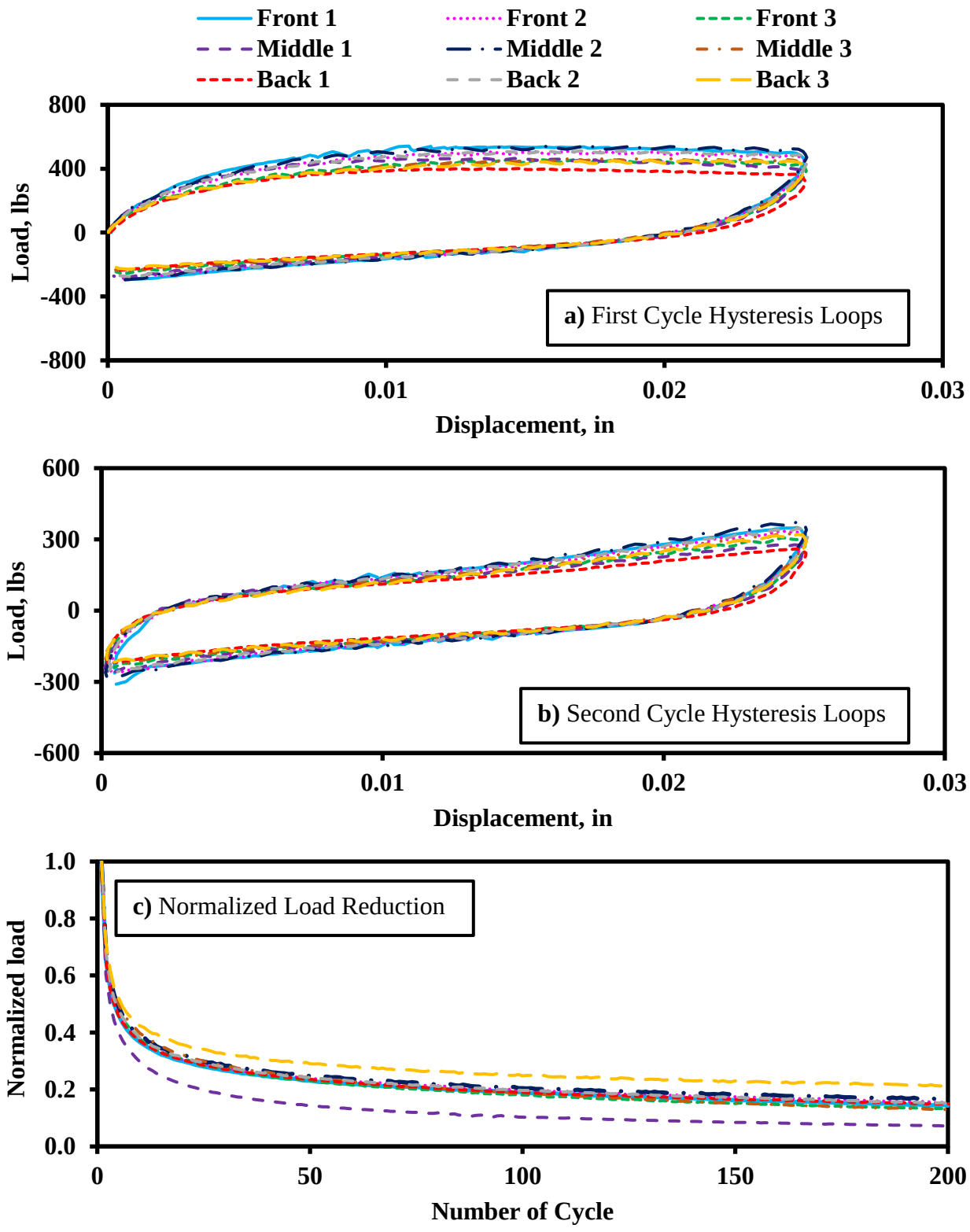

Figure 4.7: Overlay Tester Results for SMA-D Mix

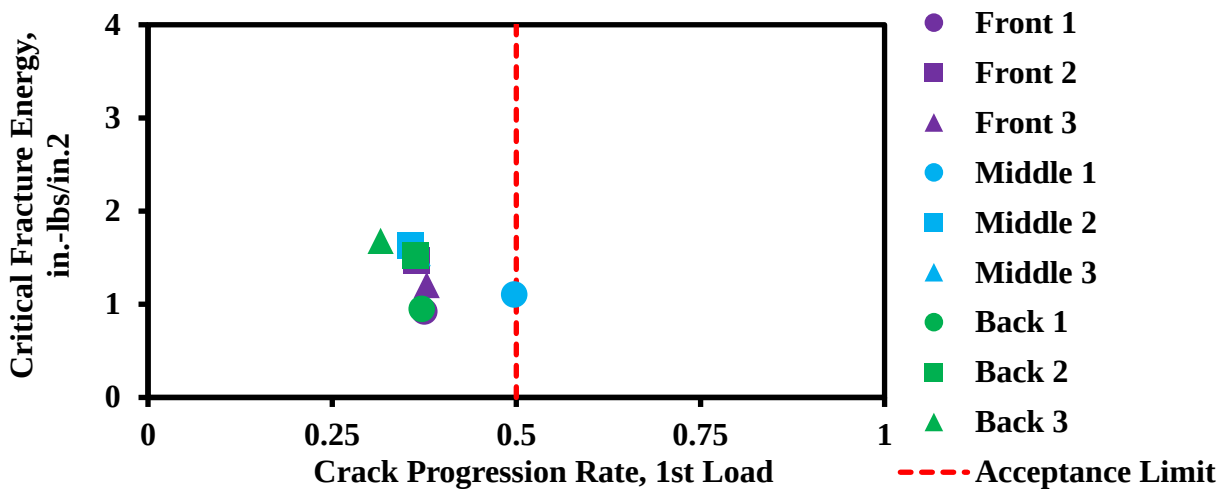

Figure 4.8: Performance of SMA-D on Design Interaction Plot

Table 4.3: Summary of OT Results for SMA-D Mix

Specimen	Air Voids, %	Max Load, lbs	Work of Fracture, in-lbs	Critical Fracture Energy, in.-lbs/in.^{2}	Crack Progression Rate	Number of Cycles to Failure
Front 1	6.0	542	4.1	0.9	0.38	200
Front 2	6.4	508	6.6	1.5	0.37	200
Front 3	7.9	457	5.4	1.2	0.38	200
Middle 1	7.1	465	5.0	1.1	0.50	200
Middle 2	5.7	541	7.3	1.6	0.36	200
Middle 3	8.0	463	7.0	1.5	0.37	200
Back 1	7.1	401	4.3	0.9	0.37	200
Back 2	6.7	511	6.8	1.5	0.36	200
Back 3	8.8	452	7.6	1.7	0.32	200
Average	7.1	482	6.0	1.3	0.38	200
Std Dev	1.0	44	1.2	0.3	0.05	0
COV	**13%**	**9%**	**21%**	**21%**	**12%**	**NA**

Table 4.4 contains an overview of the variations in the salient properties of all samples prepared for OT in this study. With COV's of 7% to 14% for the air void contents, the COV's of the critical fracture energy values and the crack progression rates for all mixes were all also more than 10%, with Type-D sample exhibiting the highest variations for most parameters extracted.

Table 4.4: Summary of OT Properties for all Mixes

Mix	Air Voids, %		Max Load, lbs		Work of Fracture, in-lbs		Critical Fracture Energy, in.-lbs/in.^{2}		Crack Progression Rate		Number of Cycles to Failure	
	Avg	COV	Avg	COV	Avg	COV	Avg	COV	Avg	COV	Avg	COV
Type-C	7.2	7	803	11	6.3	17	1.4	17	2.0	20	8	17
Type-D	7.8	10	1031	7	10.2	17	2.3	17	1.7	46	34	123
SMA-D	7.1	13	482	9	6.0	21	1.3	21	0.38	12	200	NA
TOM	7.5	14	734	10	11.0	17	2.4	17	0.42	22	150	32

4.3 Indirect Tensile Test Results

The locations of the six extracted specimens from a compacted SBC sample are shown in Figure 4.9. The load displacement curves captured for all specimens are shown in Figure 4.10. The specimens exhibited similar load-displacement curves.

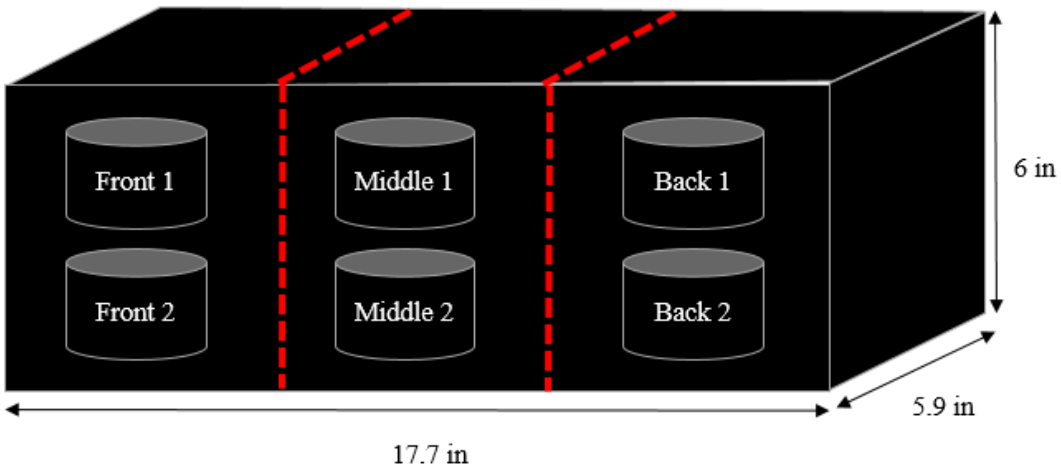

Figure 4.9: IDT extraction method

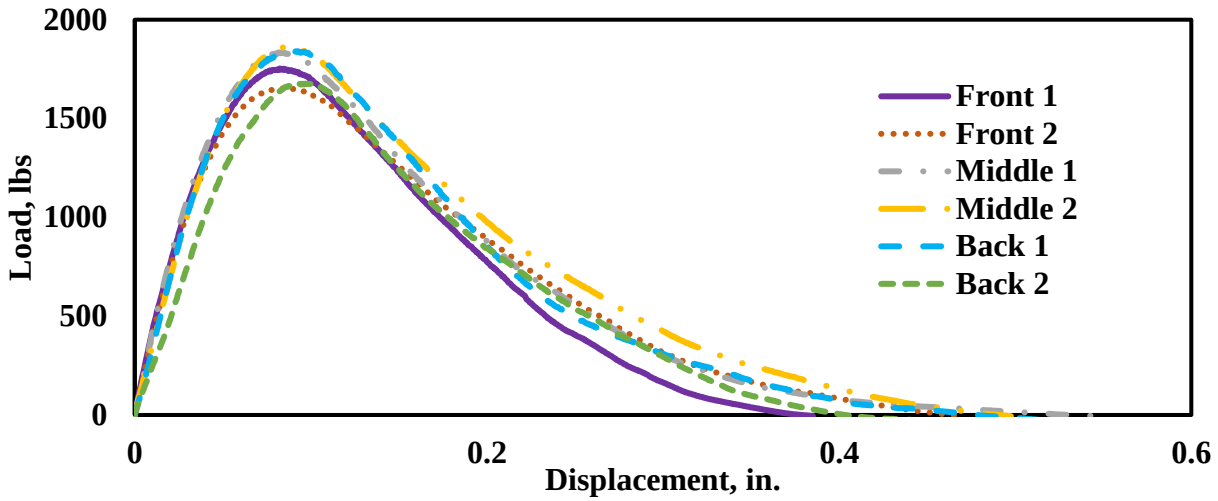

Figure 4.10: IDT Load-displacement Response Curves for SMA-D Mix

Table 4.5 provides the salient properties of each specimen, such as the calculated tensile strength and the strain at peak load. With a COV of 14% for air void content, the COV's of the extracted results varied between 6% and 7%, except the tensile modulus.

Table 4.5: Summary of IDT Results for SMA-D Mix

Specimen	Air Voids, %	Maximum Load, lbs	Tensile Modulus, psi	Tensile Strength, psi	Strain at Peak Load, %
Front 1	7.5	1753	10591	115	1.9
Front 2	10.0	1657	10561	109	2.1
Middle 1	7.3	1835	10728	121	2.0
Middle 2	7.0	1864	8796	123	2.0
Back 1	7.4	1840	9147	121	2.2
Back 2	8.5	1676	6722	110	2.3
Average	8.0	1775	9191	117	2.1
Std Dev	1.1	99	1620	7	0.1
COV	**14%**	**6%**	**18%**	**6%**	**7%**

Table 4.6 contains an overview of the variations in the salient properties of all samples prepared for IDT in this study. The COV's of the tensile strength for all mix samples were less

than 10%. The COV's of the strain at peak load for SMA-D and TOM samples were less than 10%, while the Type-C and Type-D samples were more than 10%. Again, the COV of the tensile modulus was greater than 10%.

Table 4.6: Summary of IDT Properties for all Mixes

Mix	Air Voids, %		Maximum Load, lbs		Tensile Modulus, psi		Tensile Strength, psi		Strain at Peak Load, %	
	Avg	COV	Avg	COV	Avg	COV	Avg	COV	Avg	COV
Type-C	7.7	7	1974	6	14868	18	156	6	1.6	10
Type-D	6.9	7	3685	4	24085	16	292	4	1.6	14
SMA-D	8.0	14	1775	6	9191	18	117	6	2.1	7
TOM	7.8	9	1904	5	12923	18	150	5	2.0	7

4.4 HWTD Results

The locations of the six extracted HWTD specimens from a compacted SBC sample are shown in Figure 4.11. Since two specimens are required to perform one HWTD test, specimens Front 1 and Middle 1 were paired together for one test. The maximum rut depths was captured for all specimen are illustrated in Figure 4.11. For the SMA-D mix, the back specimens' data were corrupted due to the wooden jigs lifting out of place during the testing procedure. The other two sets of specimens achieved similar rut depths.

Table 4.7 provides the salient properties of each specimen, such as the air void content and the number of passes. With a COV of 14% for air void contents, the COV at 20,000 passes was at 3%.

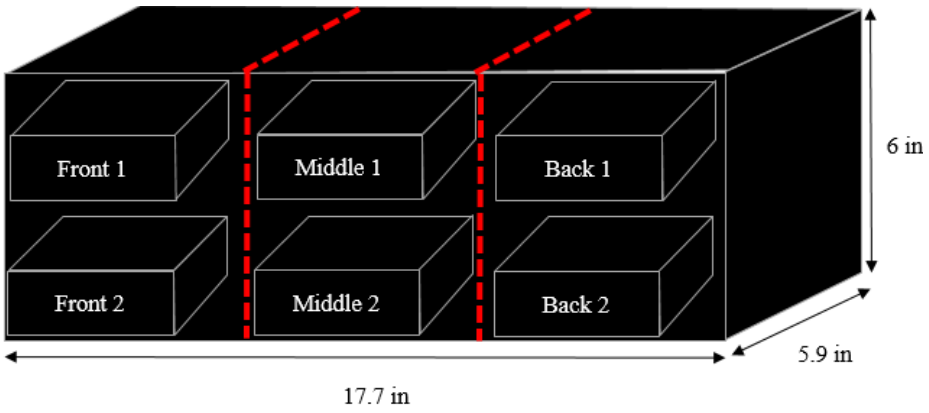

Figure 4.11: HWTD Extraction Method

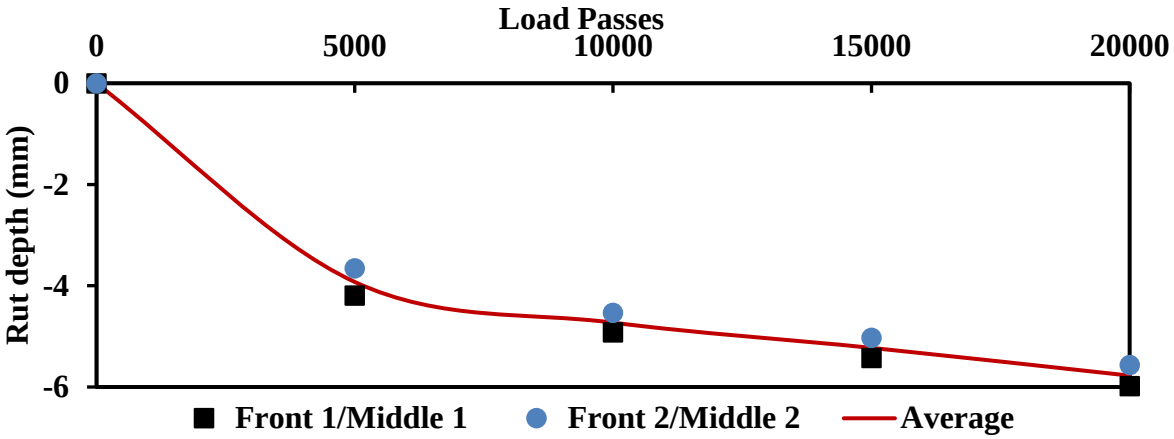

Figure 4.12: Rut Depth of Three Samples for SMA-D Mix

Table 4.7: Summary of HWTD Results for SMA-D Mix

Specimen	Air Voids, %	Rut Depth, mm after			
		5000 Passes	10000 Passes	15000 Passes	20000 Passes
Front 1	6.5	4.2	4.9	5.4	6.0
Middle 1	7.5				
Front 2	7.4	3.7	4.5	5.0	5.6
Middle 2	7.7				
Back 1	5.6	N/A*	N/A	N/A	N/A
Back 2	5.1				
Average	6.6	3.9	4.7	5.2	5.8
Std Dev	0.9	0.2	0.2	0.2	0.2
COV	**14%**	**6%**	**3%**	**3%**	**3%**

*** Back specimens' data are not available due to the wooden jigs lifting out of place during testing**

Table 4.8 contains an overview of the variations in the salient properties of all samples prepared for HWTD in this study. The COV's of the rut depth after 20,000 passes for the Type-C and SMA-D samples were less than 10%, while the Type-D and TOM samples exhibited rut depth COV's of more than 10%. From the beginning to end of the test, the COV for TOM samples had variation over 10% while SMA-D samples maintained COV's less than 10%.

Table 4.8: Summary of HWTD Properties for all Mixes

Mix	Air Voids, %		Rut Depth, mm after							
			5000 Passes		10000 Passes		15000 Passes		20000 Passes	
	Avg	COV	Avg	COV	Avg	COV	Avg	COV	Avg	COV
Type-C	7.5	2	3.1	15	4.2	6	5.2	8	6.3	9
Type-D	7.8	6	0.8	29	1.4	14	1.9	16	2.5	13
SMA-D	6.6	14	3.9	7	4.7	4	5.2	4	5.8	4
TOM	6.8	11	4.5	23	5.4	20	6	18	6.6	18

4.5 Variability of Performance Tests

The average trends from the OT results, in terms of the maximum load achieved, displacement, and the number of cycles, for all mixes are shown in Figure 4.13. The error bars in the figures demonstrate plus/minus one standard deviation from all results.

While Type-C and Type-D mixes achieved the highest average maximum loads in Figure 4.13a, both mixes averaged the lowest amount of cycles in Figure 4.13c. TOM and SMA-D attained lower maximum loads but both mixes achieved higher number of cycles. Overall, TOM and SMA-D behaved similarly and had little variation.

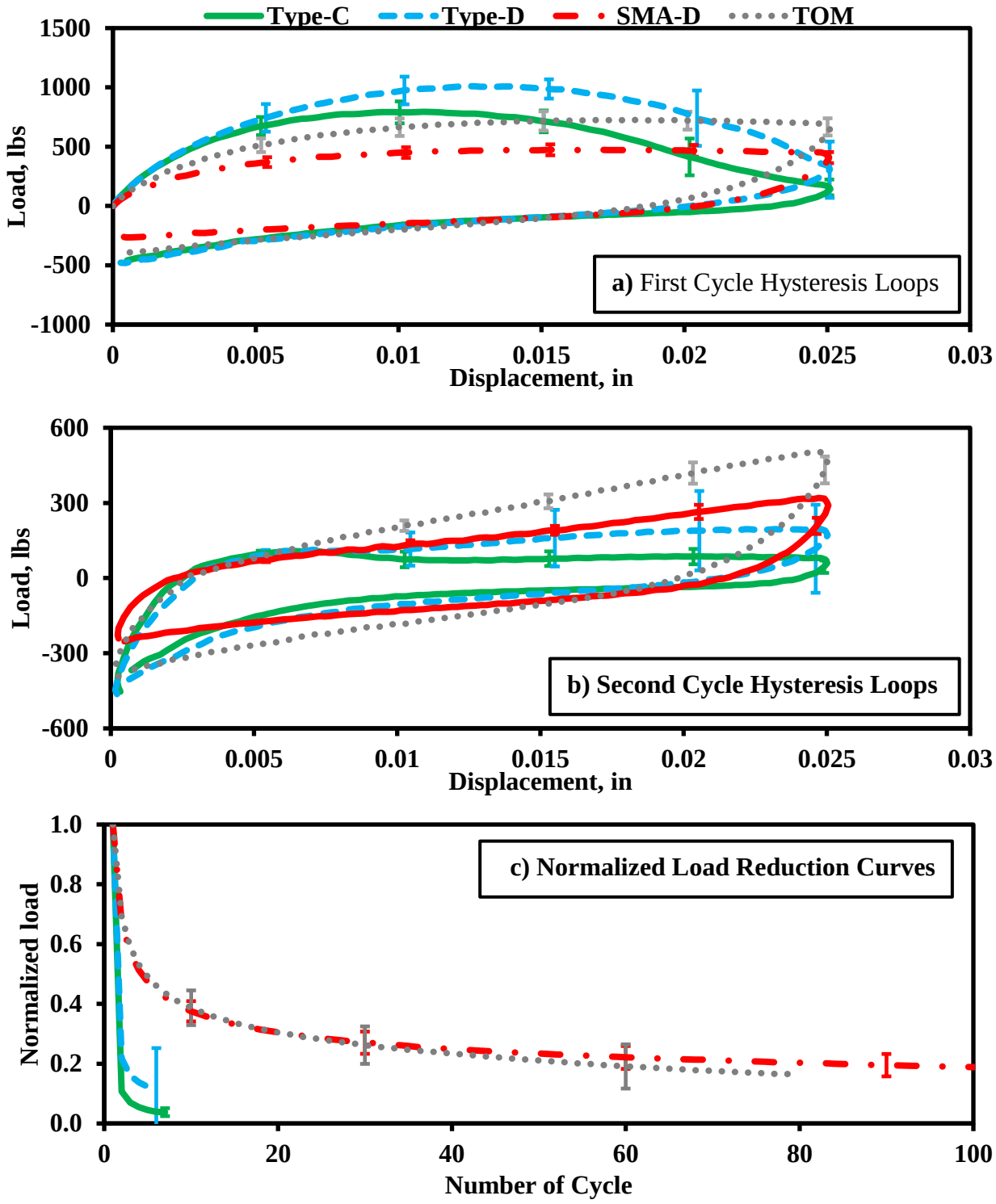

Figure 4.13: Average Overlay Tester Results for HMA Mixes

The average trends of the load-displacement curves from IDT tests are shown in Figure 4.14. All mixes achieved a similar peak load except for Type-D. TOM and SMA-D mixes again performed similarly and maintained little variation in behavior.

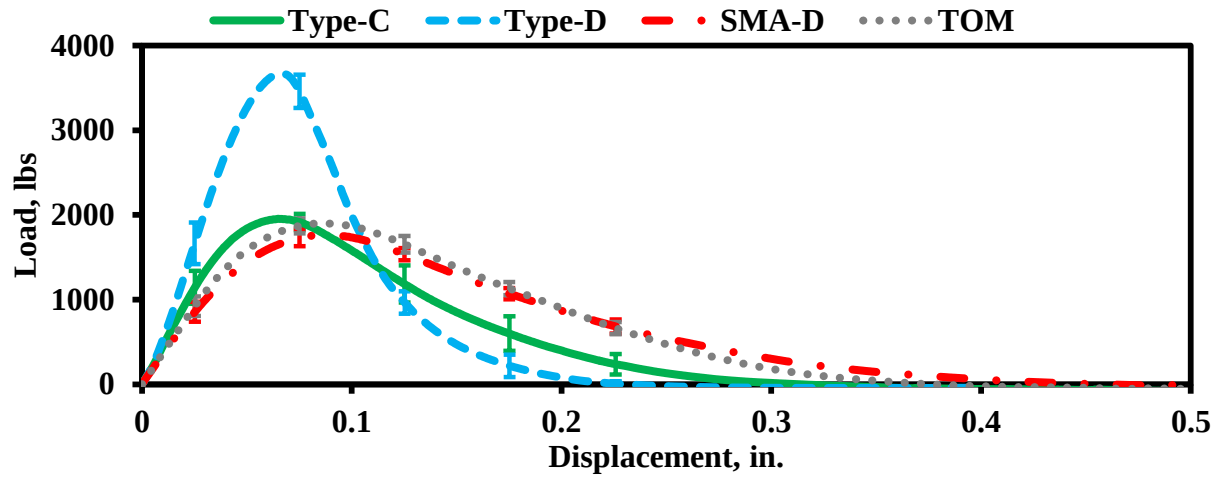

Figure 4.14: IDT Average Tensile Strength Performance Mixes Comparison

The average trends for the rut depths measured up to 20,000 passes for all mixes are shown in Figure 4.15. Type-D mix achieved the lowest amount of rut depth, while the other mixes attained similar rut depths. TOM was the mixture with the highest variation and maximum rut depth.

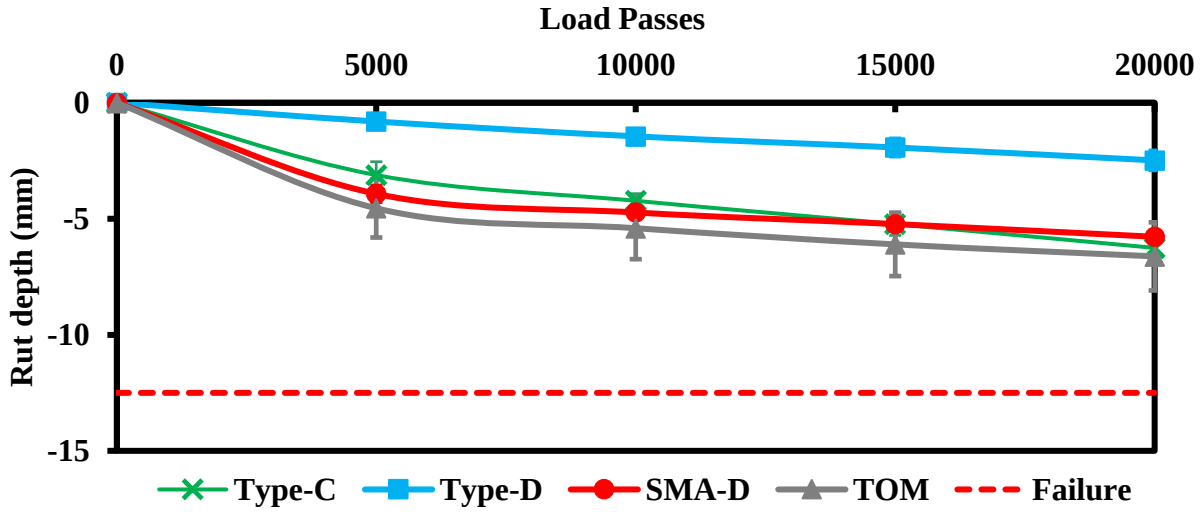

Figure 4.15: IDT Average Tensile Strength Performance Mixes Comparison

4.6 Compatibility of Results with SGC

The average air void contents for all SBC and SGC specimens are compared in Figure 4.16. Again, the error bars represent plus/minus one standard deviation. The air void contents for all the mixes tested by the SBC were above the 7% target. SMA-D and TOM mixes both had higher variability than Type-C and Type-D mixes for the SBC. The air void contents from the SGC are typically lower and closer to the 7% target with less variability.

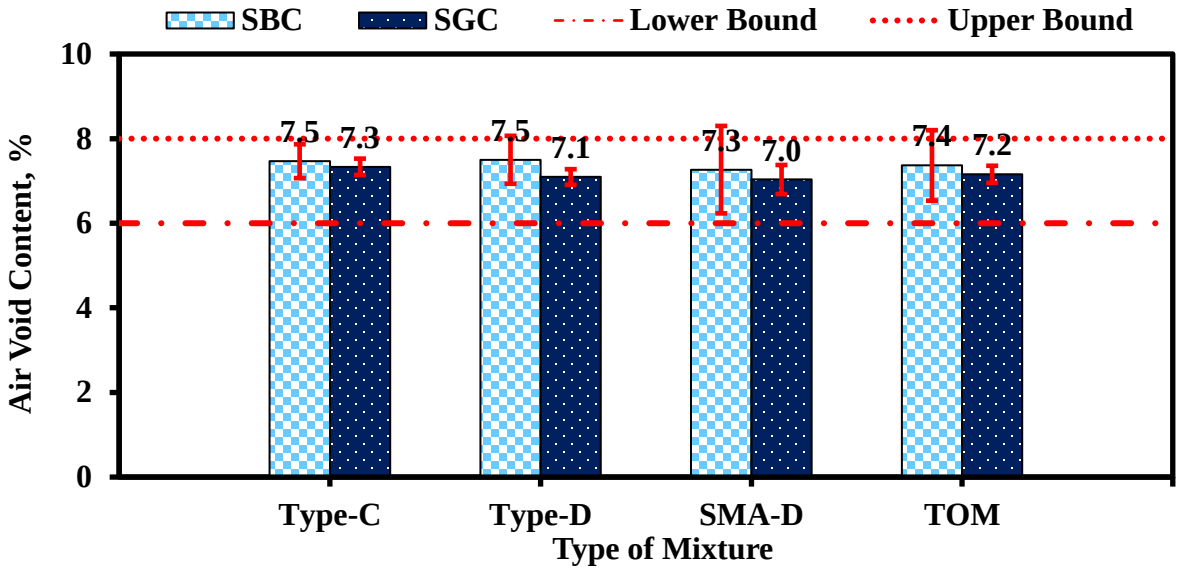

Figure 4.16: Average Air Voids for all Specimens

Figure 4.17 presents the performance of all mixes in the design interaction plot. The upper and lower limits were obtained from Garcia and Miramontes (2015). SMA-D and TOM specimens for both SBC and SGC behaved similarly with small variation. Type-C and Type-D specimens from the SBC were significantly different than those from SGC. These mixes also demonstrate large variability in the results.

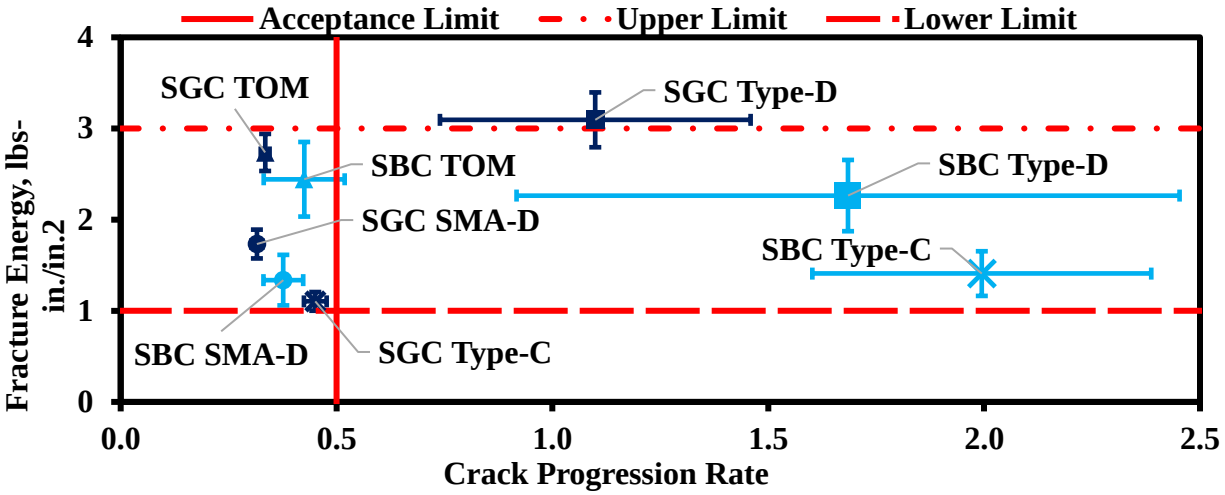

Figure 4.17: Design Interaction Plot Comparison of Mixes Performance

Figure 4.18 presents the tensile strength performance for all mixes. Current TxDOT mix design specifies a minimum and maximum allowable IDT strengths of 85 psi and 200 psi, respectively. Type-D and SMA-D SBC specimens achieved higher tensile strengths than SGC specimens. Type-D specimens exhibited higher tensile strengths than the maximum allowable strength for both SBC (significantly) and SGC (marginally). Type-C and TOM SBC and SGC specimens behaved similarly. Type-C specimens exhibited the highest variability from all mixes.

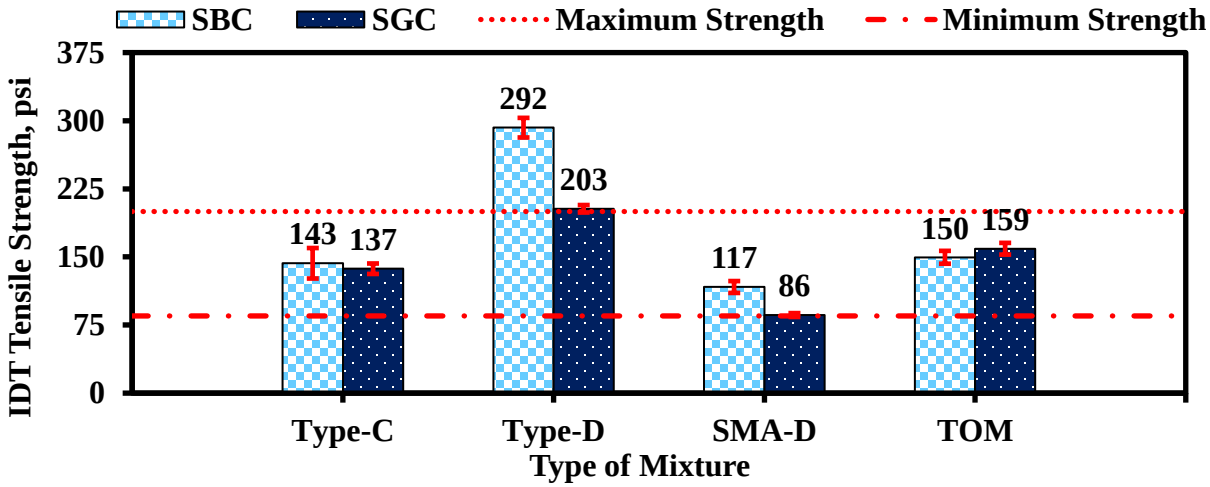

Figure 4.18: IDT Average Tensile Strength Performance Mixes Comparison

Figure 4.19 presents the rutting performance for all mixes. All SBC specimens produced higher rutting than the specimens prepared by SGC. The Type-D specimens performed the best out of all the mixes. The TOM specimens exhibited the highest variability.

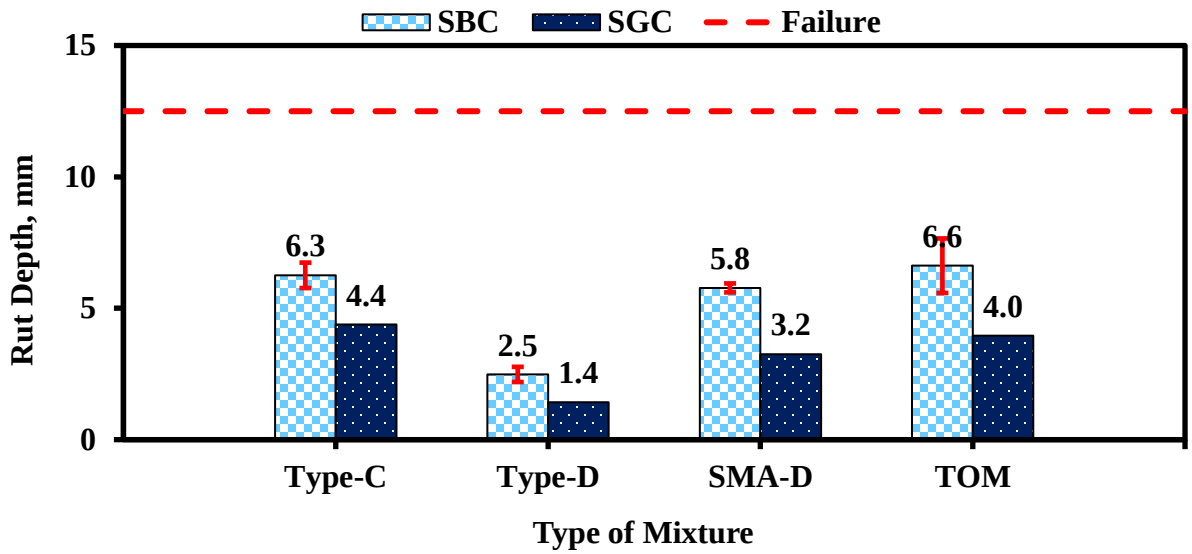

*** HWTD Specimens for SGC do not have error bars since only one sample was used for each mix**

Figure 4.19: IDT Average Rutting Depth at 20,000 passes

Chapter 5: Summary, Conclusion, and Recommendations

5.1 Summary

HMA laboratory compactors in the industry today produce adequate performance test specimens, but at present very few laboratory compactors can compact in the same manner as a roller compactor in the field compaction. The main objective of this study was to evaluate the performance of SBC as a standard compactor. This study was focused on studying the air void distribution on SBC samples and testing different performance test specimens to evaluate the repeatability of the SBC.

5.2 Conclusions

Upon the completion of testing and analyzing results with the SBC, the following observations and conclusions are presented:

- Properly preparing an SBC sample for compaction is paramount, the preparation and compaction method should be followed closely for every compaction
- From a thorough analysis of the air void contents, the COV of the air void content distribution throughout samples are about 10%
- It is important to trim the outer surface of specimens at least 0.5 – 0.8 in. (12 – 20 mm) to avoid an increase in air void content
- In terms of the mixes performance, SMA-D and TOM for OT displayed similar results with low variability to the SGC. Type-C and TOM for IDT performed similarly to SGC specimens, while SMA-D and Type-D mixtures exhibited much higher strengths. All the HMA mixes for HWTD produced much higher rutting than SGC specimens.

5.3 Recommendations

The following recommendations are suggested to further implement SBC for laboratory compaction and testing:

- Further evaluation of air void content in compacted samples with either SMA-D, TOM or similar gap graded mixture
- Implement and evaluate other types of performance test specimens extracted from SBC. In Figure 6.1 an example of a compacted sample with Disk-Shaped Compaction Test (DSCTT), Repeated Loading Direct-Tensions Test (R-DT), and Semi-Circular Bending (SCB) is shown.

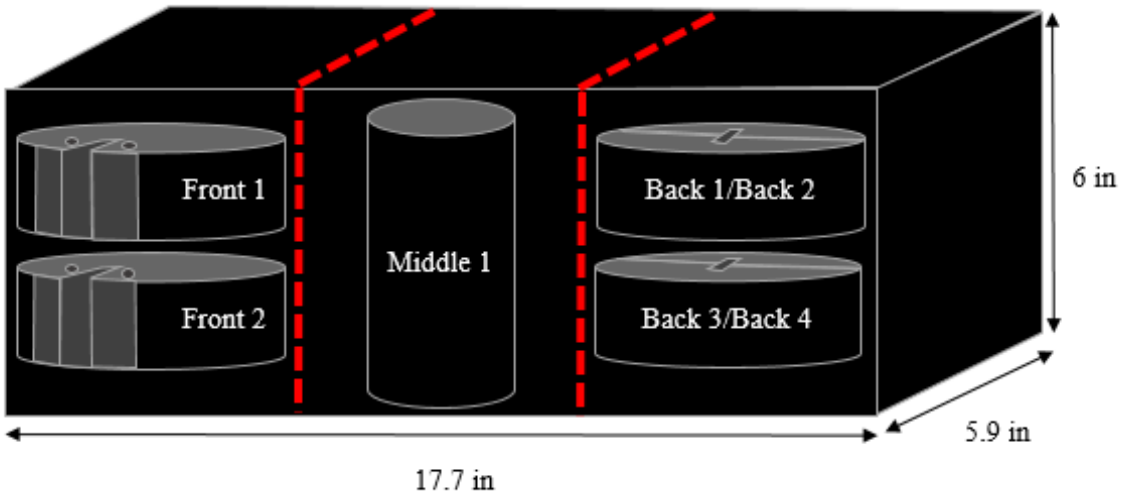

Figure 5.1: Extraction of Other Types of Performance Tests

- Conduct study on other input parameters, (height, density, vertical stress, angle of gyration), to determine how they affect SBC compaction
- Also, the modulus of the mixture can be examined depending which way the user extracts specimens from a compacted sample

References

1. Aschenbrener, T., and G. Currier. (1993) “Influence of Testing Variables on the Results from the Hamburg wheel-Tracking device.” Report No. CDOT-DTD-R-93-22, Colorado Department of Transportation, Denver.

2. ASTM International. (2015) “Standard Practice for Compaction of Prismatic Asphalt Specimens by Means of the Shear Box Compactor.” ASTM D7981-15, ASTM International, West Conshohocken, PA

3. Bennert, T. and Ali, M. (2008). “Field and Laboratory Evaluation of a Reflective Crack Interlayer in New Jersey,” Journal of the Transportation Research Board, No. 2084, 2008, pp. 112-123, Transportation Research Board of the National Academies, Washington, D.C.

4. Gabrawy, T. (2000). “Towards laboratory replication of field compaction: asphalt shear box compactor”, Proceedings World of Asphalt Pavements International Conference, Australian Asphalt Pavements Association, Sydney, Australia.

5. Garcia, V. and A. Miramontes. (2015) "Understanding Sources of Variability of Overlay Test Procedure." No. 16-2317, Journal of the Transportation Research Board, No. 2507, pp. 10-18, Transportation Research Board of the National Academies, Washington, D.C.

6. Harman, T., Bukowski, J.R., Moutier, F., Huber, G., and McGennis, R. (2002) “The History and Future Challenges of Gyratory Compaction 1939 to 2001,” No. 02-2512, Journal of the Transportation Research Board , No. 1789, pp. 200-207, Transportation Research Board of the National Academies, Washington, D.C.

7. Hajj, E., Sebaaly, P., Porras, J., and Azofeifa, J. (2010). “Reflective Cracking of Flexible Pavements Phase III: Field Verification.” Research Report No. 13KJ-1, Nevada Department of Transportation, Research Division, University of Nevada, Reno.

8. Kennedy, T. W. and Anagnos, J. N. (1983) “Method for Conducting the Static and Repeated Load Indirect Tensile Test,” Research Report 183-15F, Center for Transportation Research, The University of Texas at Austin, Texas

9. Khan, Z. A., Wahab, H. I., Asi, I., and Ramadhan, R. (1998) “Comparative Study of Asphalt Concrete Laboratory Compaction Methods to Simulate Field Compaction,” Construction Building Materials No. 6-7, Vol. 12, pp. 373–384, Center for Engineering Research, Research Institute, King Fahd University of Petroleum and Minerals, Saudi Arabia

10. Lu, Q., Luo, S., Harvey, J. (2011) “Compaction of Noise-Reducing Asphalt Mixes in the Laboratory.” Geotechnical Special Publication No. 213, pp. 97-105, American Society of Engineers, New York, NY

11. McRae, J. L. (1965) “Theoretical Aspects of Asphalt Concrete Mix Design,” Proceedings, 3rd Paving Conference, Civil Engineering Department, the University of New Mexico, Albuquerque, New Mexico

12. Qiu, J., Xuan, D., van de Ven, M. F. C., and Molenaar, A. A. A. (2009) “Evaluation of the Shear Box Compactor as an Alternative Compactor for Asphalt Mixture Beam Specimens,” AES-ATEMA 2009 3rd International Conference on Advances and Trends in Engineering Materials and Their Applications, July 06–10, 2009, Advanced Engineering Solutions, Montreal, Canada.

13. Qiu, J., N. Li, F. P. Pramesti, M. F. van de Ven, and A. A. Molenaar. (2012) "Evaluating Laboratory Compaction of Asphalt Mixtures Using the Shear Box Compactor." Journal of Testing and Evaluation, Vol. 40, No. 5, pp. 844-852, ASTM International, West Conshohocken, PA

14. Romero, F.L., and K.D. Stuart (1998). “Evaluating Accelerated Rut Testers.” Public Roads, Vol. 62, No.1, July-August., pp 50-54, Federal Highway Administration, U.S. Department of Transportation, Washington, D.C.

15. D. Swiertz, E. Mahmoud, H. Bahia (2010) “Asphalt mixture compaction and aggregate structure analysis techniques: state of the art report,” RILEM Technical Committee 206-ATB Meeting, Transportation Research Board, Washington, D.C.

16. Walubita, L. F., Faruk, A. N., Koohi, Y., Luo, R., and Scullion, T. (2013). “The Overlay Tester (OT): Comparison with Other Crack Test Methods and Recommendations for Surrogate Crack Tests.” Research Report FHWA/TX-13/0-6607-2. Texas Transportation Institute, Texas A&M University System, College Station, Texas.

17. Walubita, L.F., A. N. M. Faruk, G. Das, H. A. Tanvir, J. Zhang, T. Scullion (2012). “The Overlay Tester: A Sensitivity Study to Improve Repeatability and Minimize Variability in the OT Test Results.” Research Report FHWA/TX-12/0-6607-1. Texas Transportation Institute, Texas A&M University System, College Station, Texas.

18. Zhou, F., Hu, S., and Scullion, T. (2006). “Integrated asphalt (overlay) mixture design, balancing rutting and cracking requirements.” FHWA/TX-06/0-5123-1, Texas Transportation Institute, College Station, Texas.

19. Zhou, F., and Scullion, T. (2003) “Upgraded overlay tester and its application to characterize reflection cracking resistance of asphalt mixtures” FHWA/ TX-04/0-4467-1, Texas Transportation Institute, College Station, Texas.

Appendix A: Results with the SBC

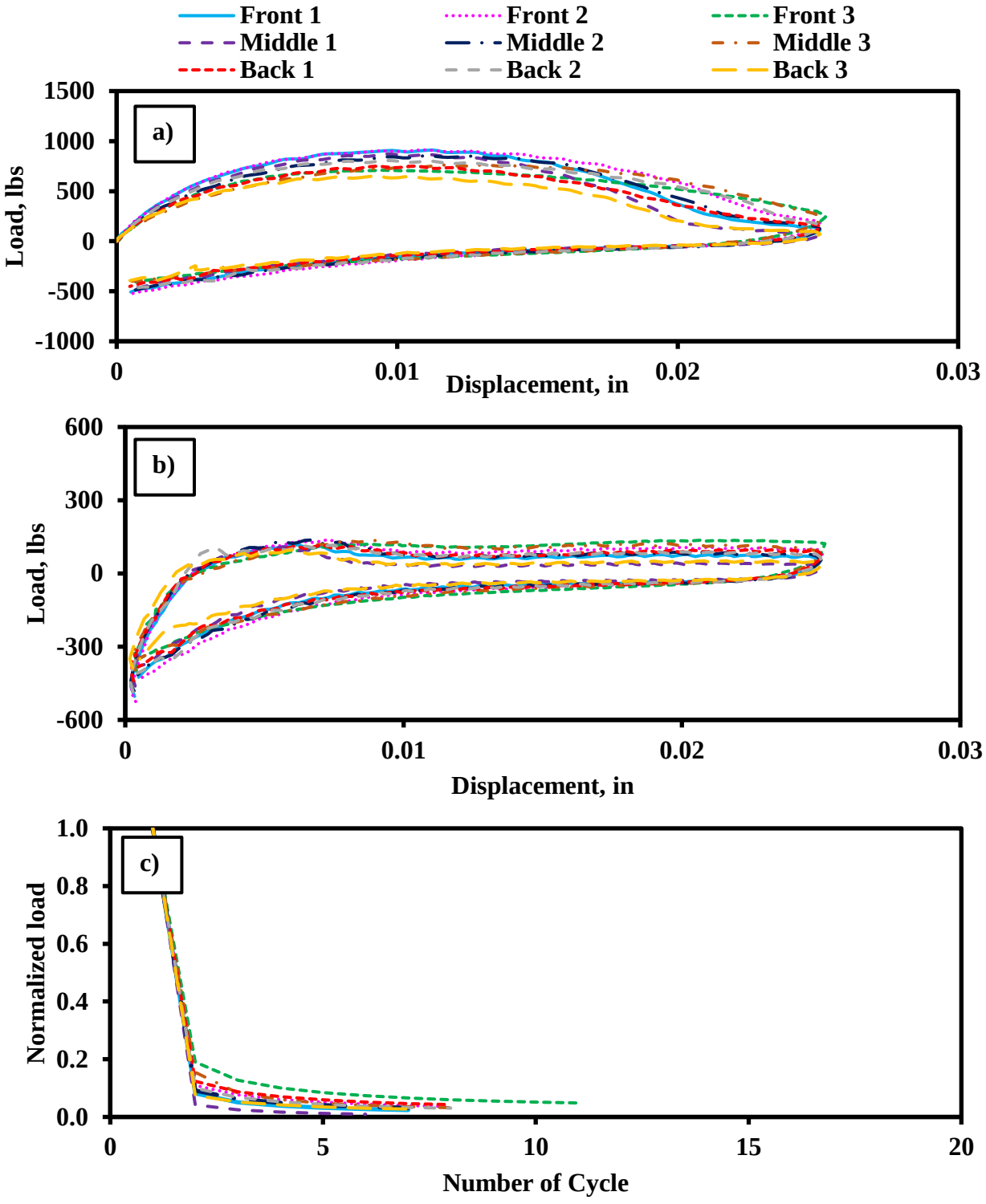

Figure A1: Results for Type-C Mix: a) First Cycle Hysteresis Loop, b) Second Cycle Hysteresis Loop, and c) Normalized Load Reduction Curves

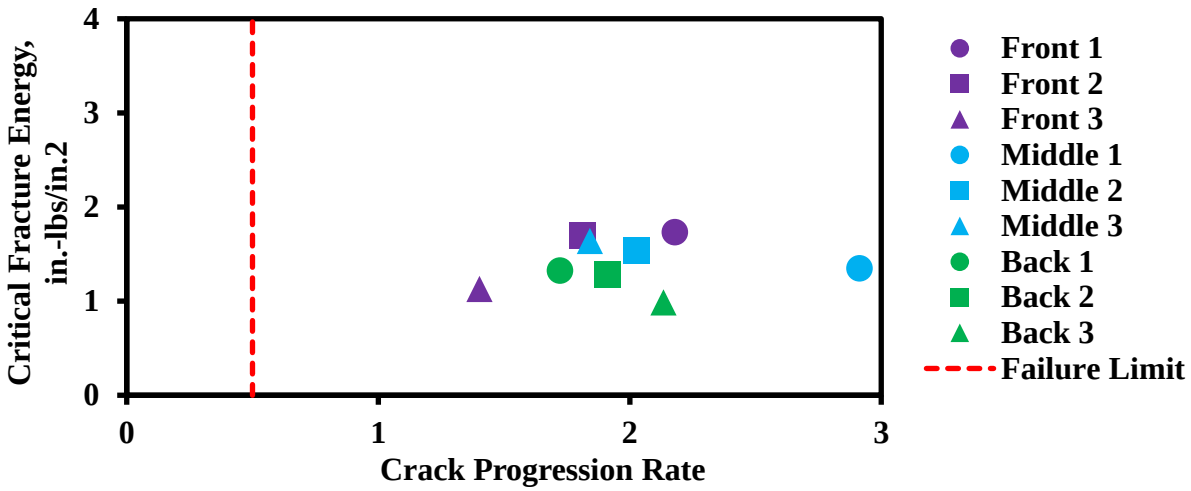

Figure A2: Performance of Type-C on Design Interaction Plot

Table A1: Summary of OT Results for Type-C Mix

Specimen	Air Voids, %	Max Load, lbs	Work of Fracture, in-lbs	Critical Fracture Energy, in.-lbs/in.^{2}	Crack Progression Rate	R^2	Number of Cycles to Failure
Front 1	7.0	911	7.8	1.7	2.18	0.97	7
Front 2	6.6	912	7.6	1.7	1.81	0.97	8
Front 3	8.0	709	5.1	1.1	1.40	0.98	11
Middle 1	6.9	872	6.1	1.3	2.91	0.98	6
Middle 2	6.2	855	6.9	1.5	2.03	0.97	7
Middle 3	7.4	762	7.4	1.6	1.84	0.99	8
Back 1	7.6	751	6.0	1.3	1.72	0.97	8
Back 2	7.4	807	5.8	1.3	1.91	0.97	8
Back 3	7.6	650	4.4	1.0	2.13	0.97	7
Average	7.2	803	6.3	1.4	1.99	1.0	8
Std Dev	0.5	87	1.1	0.2	0.39	0.01	1
COV	**7%**	**11%**	**17%**	**17%**	**20%**	**1%**	**17%**

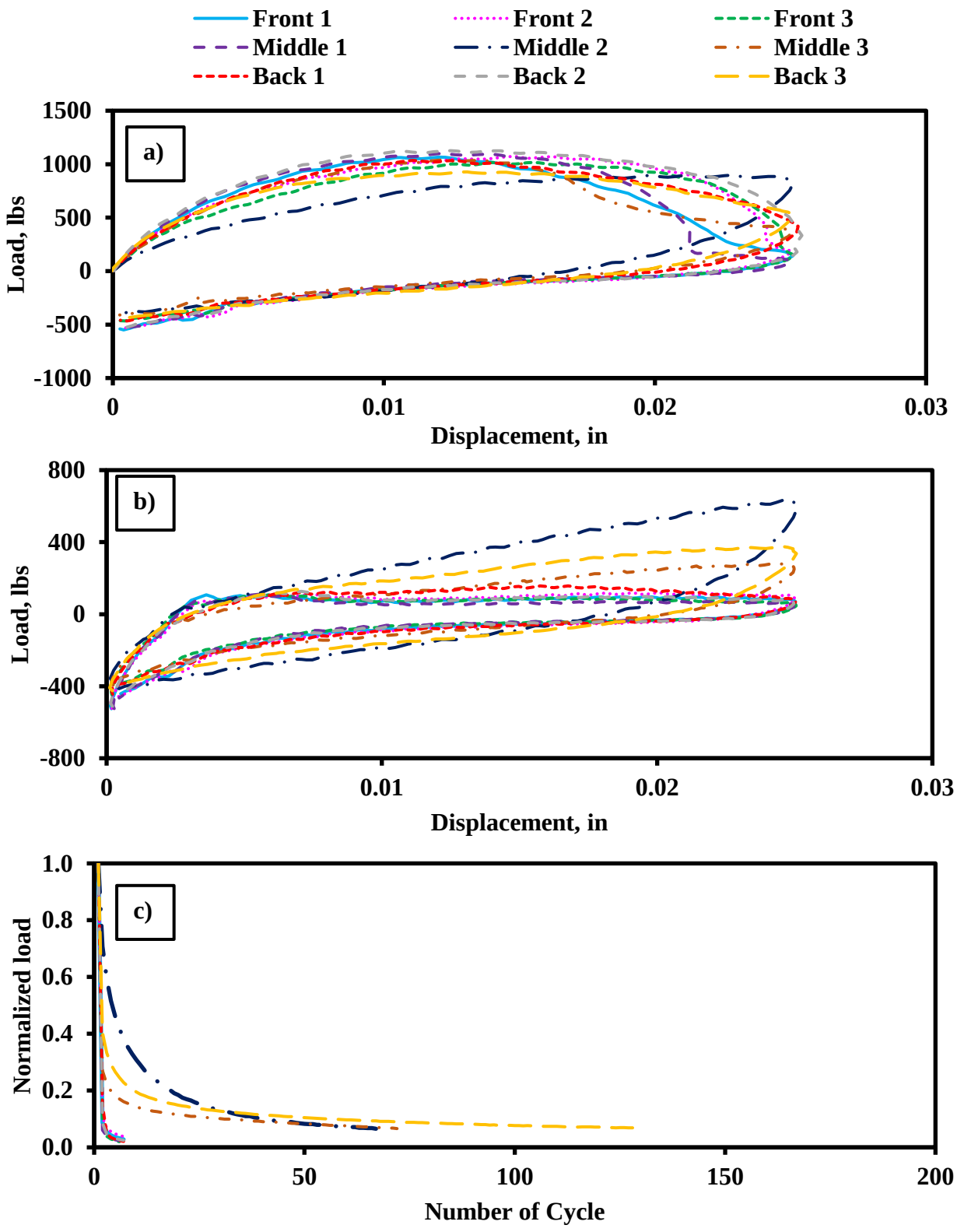

Figure A3: Results for Type-D Mix: a) First Cycle Hysteresis Loop, b) Second Cycle Hysteresis Loop, and c) Normalized Load Reduction Curves

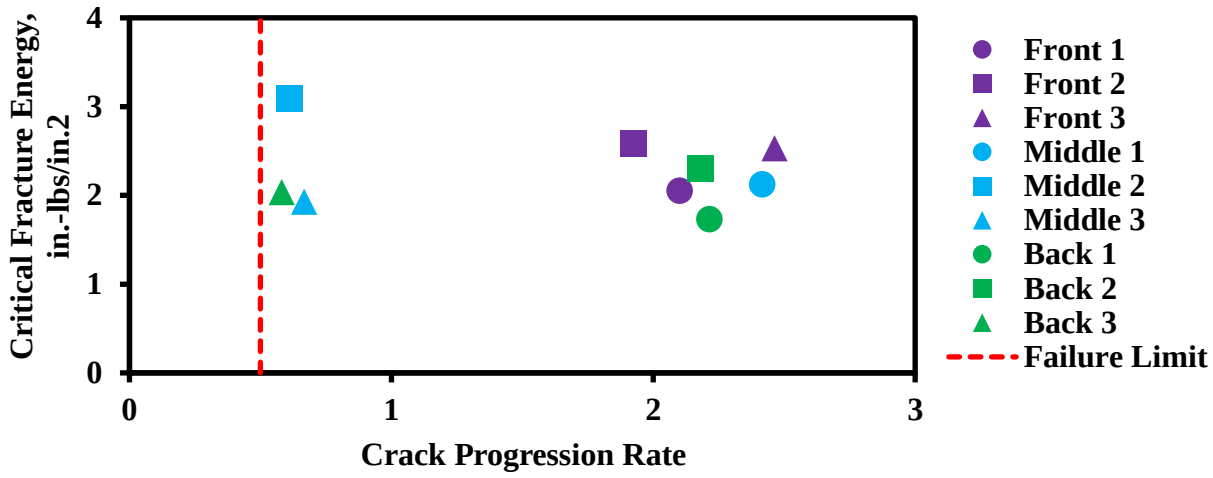

Figure A4: Performance of Type-D on Design Interaction Plot

Table A2: Summary of OT Results for Type-D Mix

Specimen	Air Voids, %	Max Load, lbs	Work of Fracture, in-lbs	Critical Fracture Energy, in.-lbs/in.^{2}	Crack Progression Rate	R^2	Number of Cycles to Failure
Front 1	8.4	1066	9.2	2.1	2.10	0.97	7
Front 2	7.4	1071	11.6	2.6	1.93	0.97	7
Front 3	8.9	1016	11.4	2.5	2.46	0.98	6
Middle 1	7.2	1099	9.6	2.1	2.42	0.96	6
Middle 2	6.4	898	13.9	3.1	0.61	1.00	67
Middle 3	8.0	1038	8.7	1.9	0.67	0.99	72
Back 1	8.0	1035	7.8	1.7	2.21	0.99	7
Back 2	7.2	1126	10.3	2.3	2.18	0.97	7
Back 3	8.6	928	9.2	2.0	0.58	1.00	128
Average	7.8	1031	10.2	2.3	1.68	1.0	34
Std Dev	0.8	71	1.8	0.4	0.77	0.01	42
COV	**10%**	**7%**	**17%**	**17%**	**46%**	**1%**	**123%**

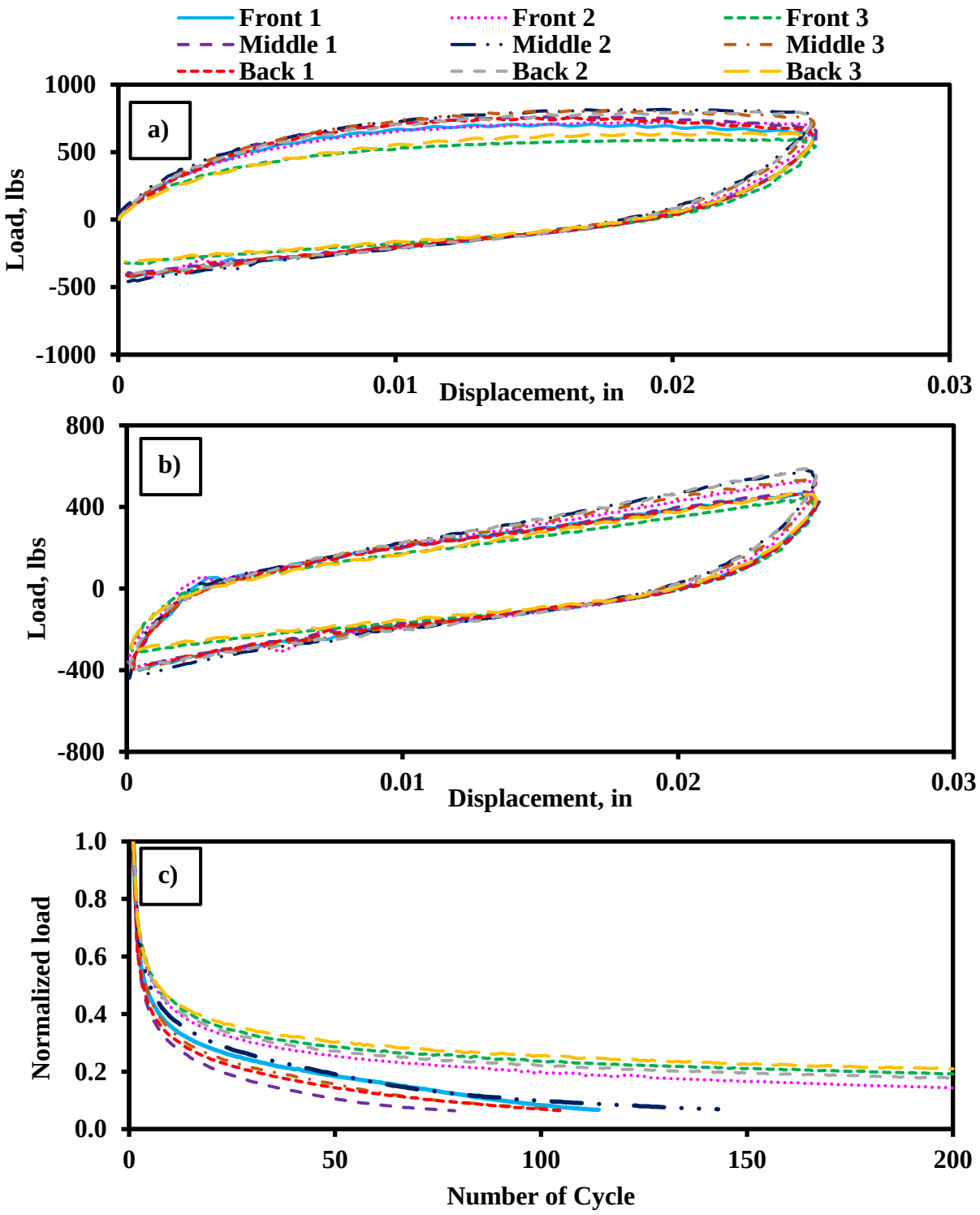

Figure A5: Results for Type-D Mix: a) First Cycle Hysteresis Loop, b) Second Cycle Hysteresis Loop, and c) Normalized Load Reduction Curves

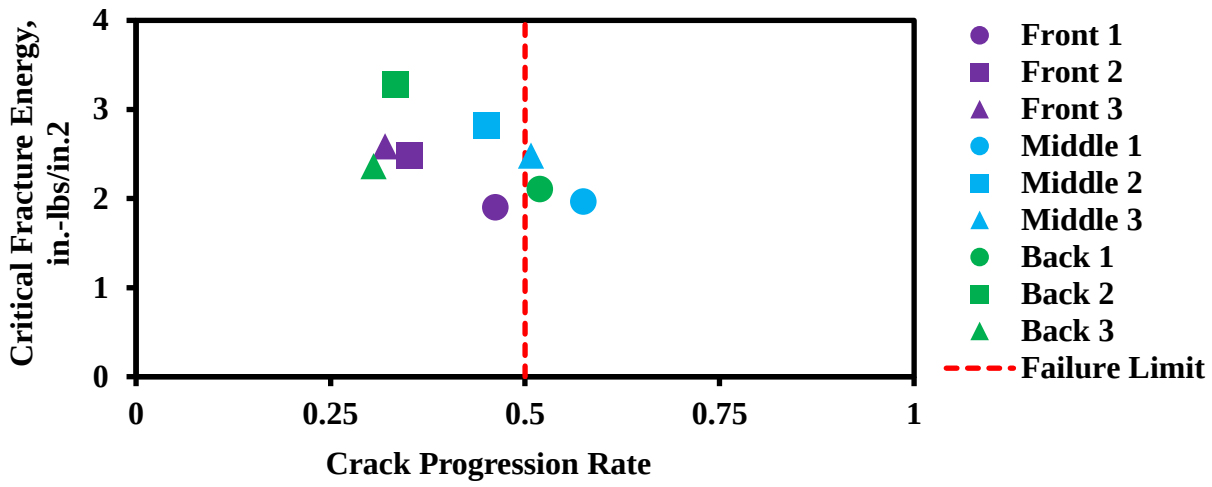

Figure A6: Performance of TOM on Design Interaction Plot

Table A3: Summary of OT Results for TOM Mix

Specimen	Air Voids, %	Max Load, lbs	Work of Fracture, in-lbs	Critical Fracture Energy, in.-lbs/in.^{2}	Crack Progression Rate	R^2	Number of Cycles to Failure
Front 1	8.0	707	8.6	1.9	0.46	0.99	114
Front 2	7.6	721	11.2	2.5	0.35	1.00	200
Front 3	9.5	597	11.6	2.6	0.32	1.00	200
Middle 1	6.9	760	8.8	2.0	0.58	1.00	79
Middle 2	6.5	816	12.7	2.8	0.45	0.99	143
Middle 3	8.5	809	11.2	2.5	0.51	0.99	107
Back 1	6.6	755	9.5	2.1	0.52	1.00	106
Back 2	6.0	799	14.8	3.3	0.33	1.00	200
Back 3	8.0	643	10.6	2.4	0.31	1.00	200
Average	7.5	734	11.0	2.4	0.42	1.00	149
Std Dev	1.1	71	1.8	0.4	0.09	0.00	47
COV	**14%**	**10%**	**17%**	**17%**	**22%**	**NA**	**32%**

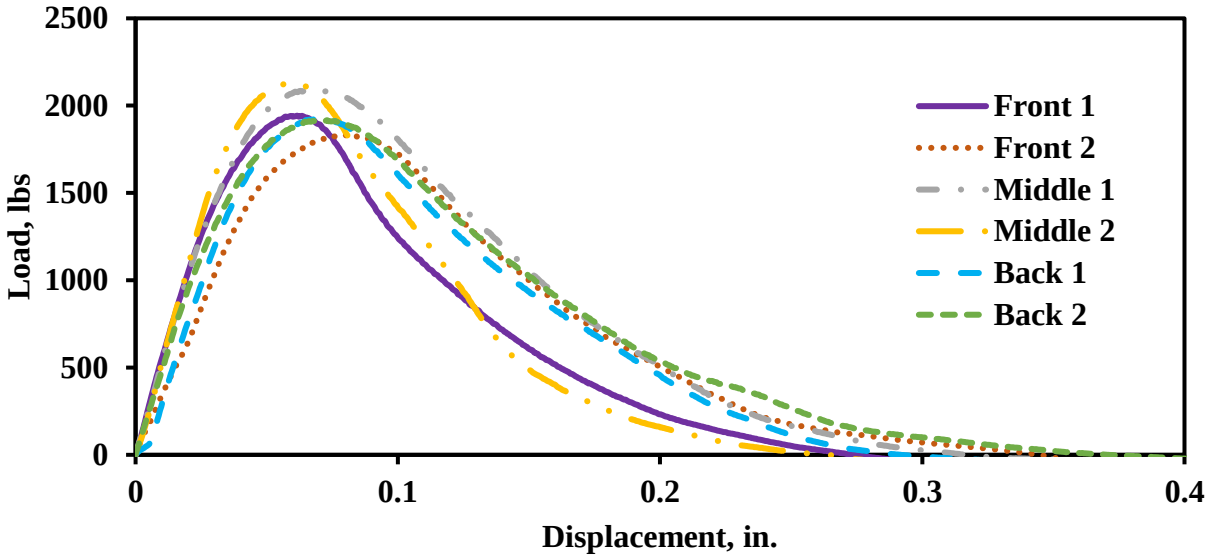

Figure A7: IDT Load-displacement Response Curves for Type-C Mix

Table A4: Summary of IDT Results for Type-C Mix

Specimen	Air Voids, %	Maximum Load, lbs	Tensile Modulus, psi	Tensile Strength, psi	Strain at Peak Load, %
Front 1	8.3	1942	16025	153	1.4
Front 2	8.2	1833	10113	145	1.8
Middle 1	7.0	2093	16153	165	1.5
Middle 2	7.2	2130	17839	168	1.4
Back 1	7.6	1929	14295	153	1.6
Back 2	7.6	1916	14783	151	1.7
Average	7.7	1974	14868	156	2
Std Dev	0.5	114	2637	9	0.2
COV	**7%**	**6%**	**18%**	**6%**	**10%**

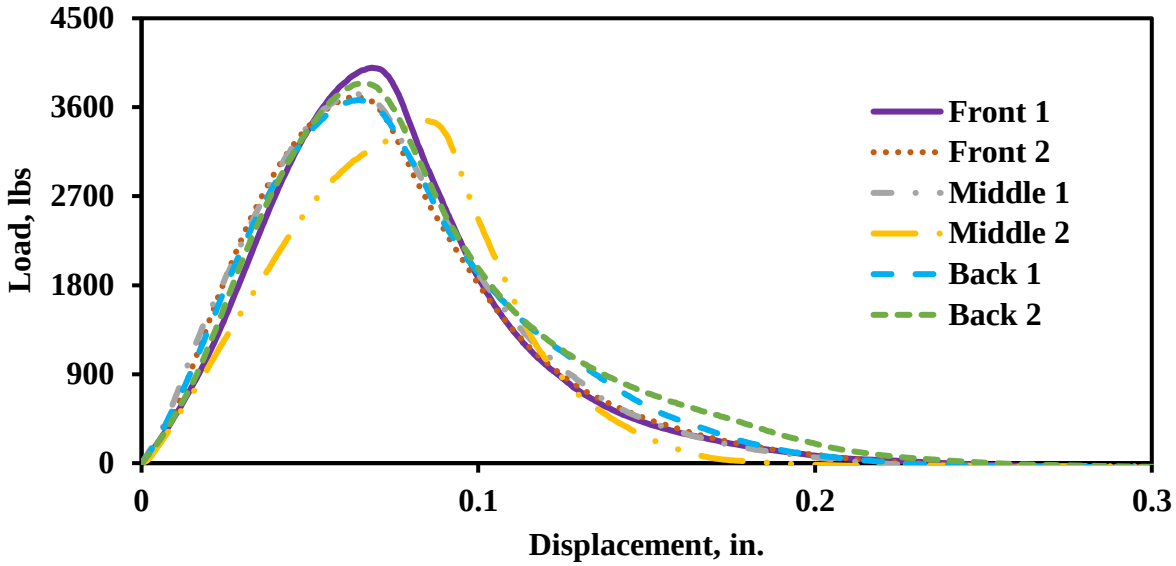

Figure A8: IDT Load-displacement Response Curves for Type-D Mix

Table A5: Summary of IDT Results for Type-D Mix

Specimen	Air Voids, %	Maximum Load, lbs	Tensile Modulus, psi	Tensile Strength, psi	Strain at Peak Load, %
Front 1	6.2	4000	24678	317	1.6
Front 2	7.1	3712	27689	294	1.5
Middle 1	6.7	3733	25125	296	1.5
Middle 2	7.7	3463	17666	275	2.0
Back 1	6.8	3675	25052	291	1.5
Back 2	7.1	3846	24895	305	1.5
Average	6.9	3685	24085	292	1.6
Std Dev	0.5	140	3770	11	0.2
COV	**7%**	**4%**	**16%**	**4%**	**14%**

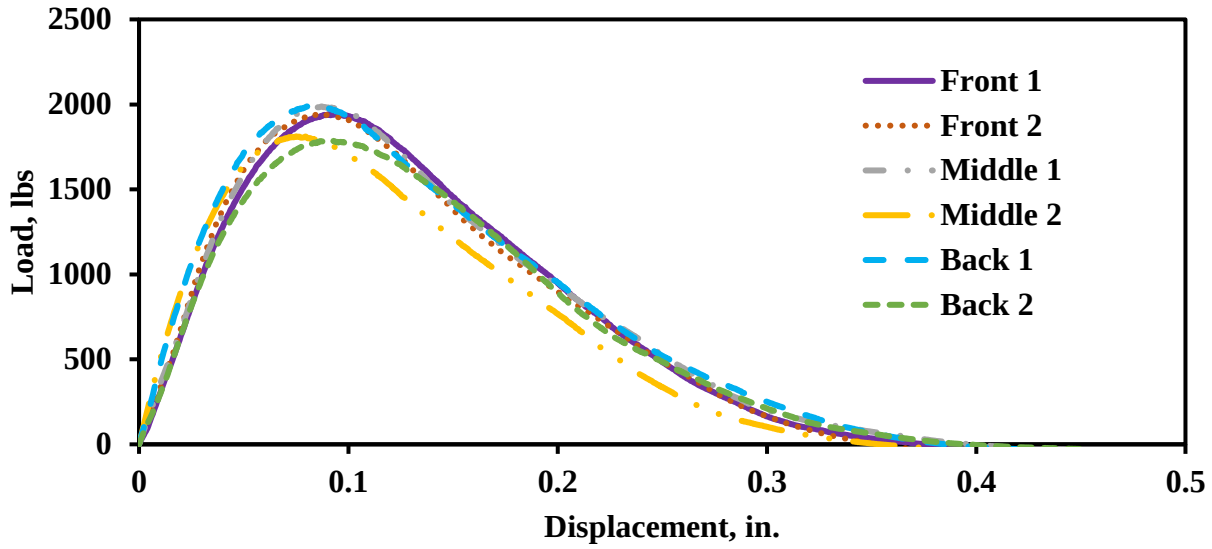

Figure A9: IDT Load-displacement Response Curves for TOM Mix

Table A6: Summary of IDT Results for TOM Mix

Specimen	Air Voids, %	Maximum Load, lbs	Tensile Modulus, psi	Tensile Strength, psi	Strain at Peak Load, %
Front 1	7.6	1945	10918	154	2.2
Front 2	8.7	1942	11678	153	2.0
Middle 1	6.9	1988	11678	153	2.0
Middle 2	8.3	1812	15863	143	1.8
Back 1	7.3	1991	14790	157	2.0
Back 2	8.0	1786	10607	141	2.2
Average	7.8	1904	12923	150	2.0
Std Dev	0.7	98	2269	7	0.1
COV	**9%**	**5%**	**18%**	**5%**	**7%**

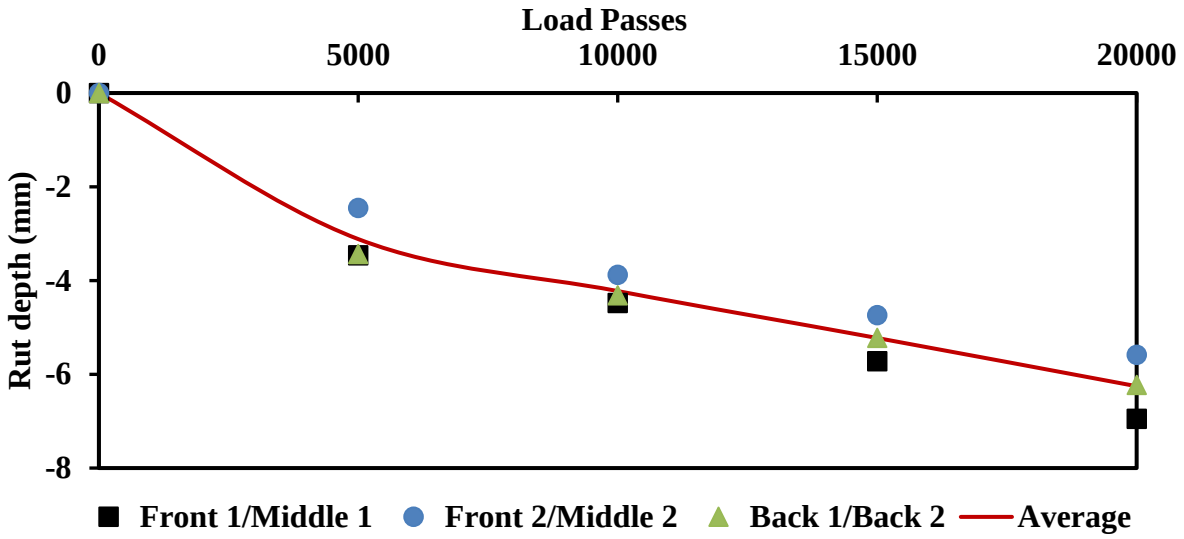

Figure A10: Rut Depth of Three Samples for Type-C Mix

Table A7: Summary of HWTD Results for Type-C Mix

		Passes				
Specimen	**Air Voids, %**	**5000**	**10000**	**15000**	**20000**	
Front 1	7.4	3.5	4.5	5.7	7.0	**Rut Depth, mm**
Middle 1	7.2					
Front 2	7.6	2.5	3.9	4.7	5.6	
Middle 2	7.7					
Back 1	7.6	3.4	4.3	5.2	6.2	
Back 2	7.5					
Average	7.5	3.1	4.2	5.2	6.3	
Std Dev	0.1	0.4	0.2	0.3	0.5	
COV	**2%**	**13%**	**5%**	**7%**	**8%**	

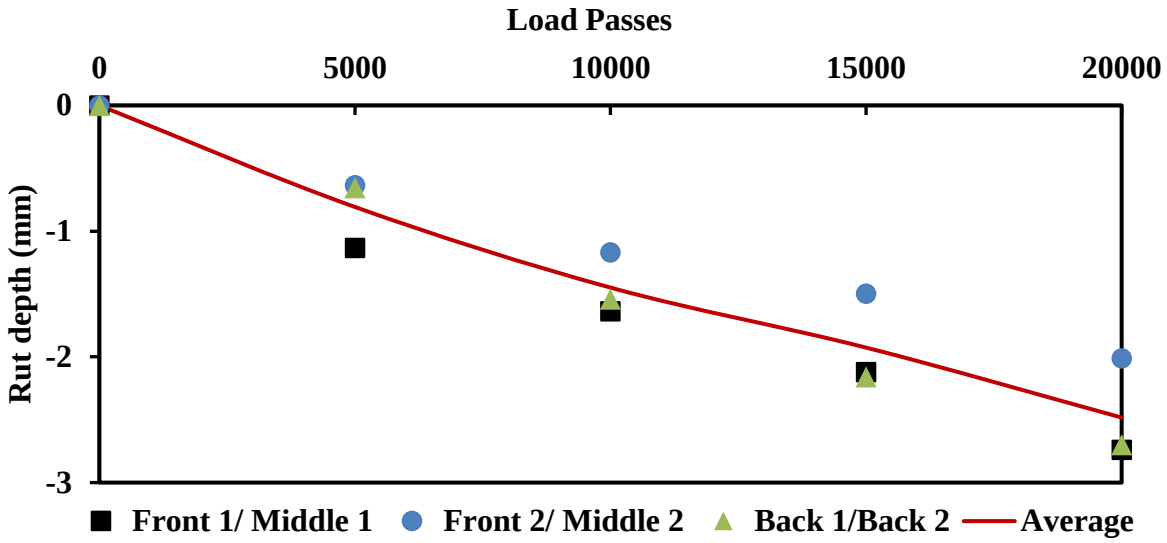

Figure A11: Rut Depth of Three Samples for Type-D Mix

Table A8: Summary of HWTD Results for Type-D Mix

		Passes				
Specimen	**Air Voids, %**	**5000**	**10000**	**15000**	**20000**	
Front 1	7.5	1.1	1.6	2.1	2.7	**Rut Depth, mm**
Middle 1	6.9					
Front 2	8.5	0.6	1.2	1.5	2.0	
Middle 2	8.0					
Back 1	7.6	0.7	1.5	2.2	2.7	
Back 2	8.3					
Average	7.8	0.8	1.4	1.9	2.5	
Std Dev	0.5	0.2	0.2	0.3	0.3	
COV	**6%**	**25%**	**12%**	**14%**	**12%**	

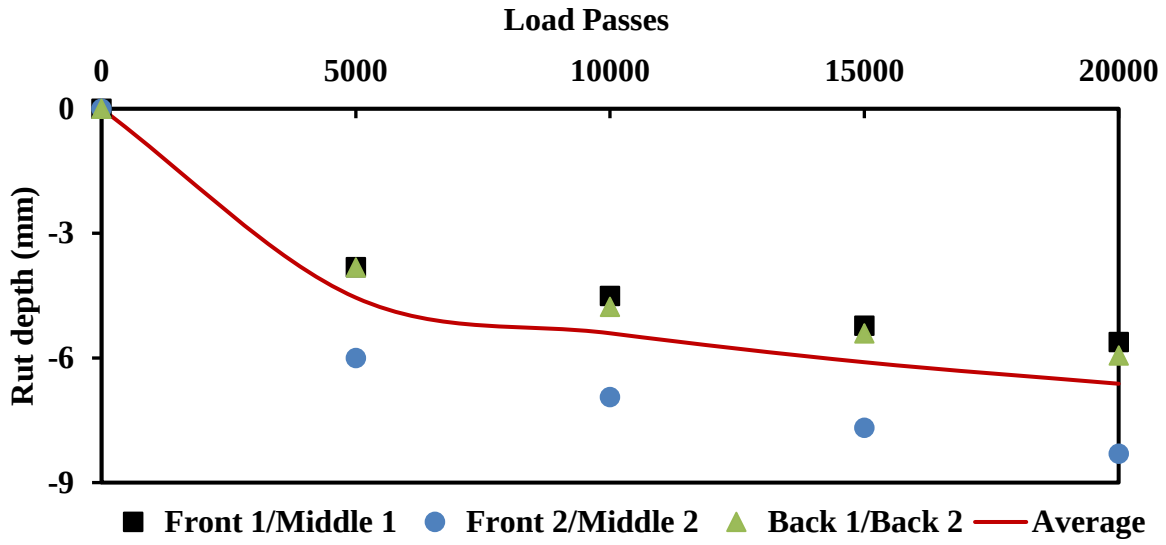

Figure A12: Rut Depth of Three Samples for TOM Mix

Table A9: Summary of HWTD Results for TOM Mix

		Passes				
Specimen	**Air Voids, %**	**5000**	**10000**	**15000**	**20000**	
Front 1	6.2	3.8	4.5	5.2	5.6	**Rut Depth, mm**
Middle 1	5.6					
Front 2	7.0	6.0	6.9	7.7	8.3	
Middle 2	7.5					
Back 1	6.5	3.8	4.8	5.4	5.9	
Back 2	7.9					
Average	6.8	4.5	5.4	6.1	6.6	
Std Dev	0.7	0.9	0.9	1.0	1.0	
COV	**11%**	**20%**	**20%**	**16%**	**16%**	

Appendix B: Results with the SGC

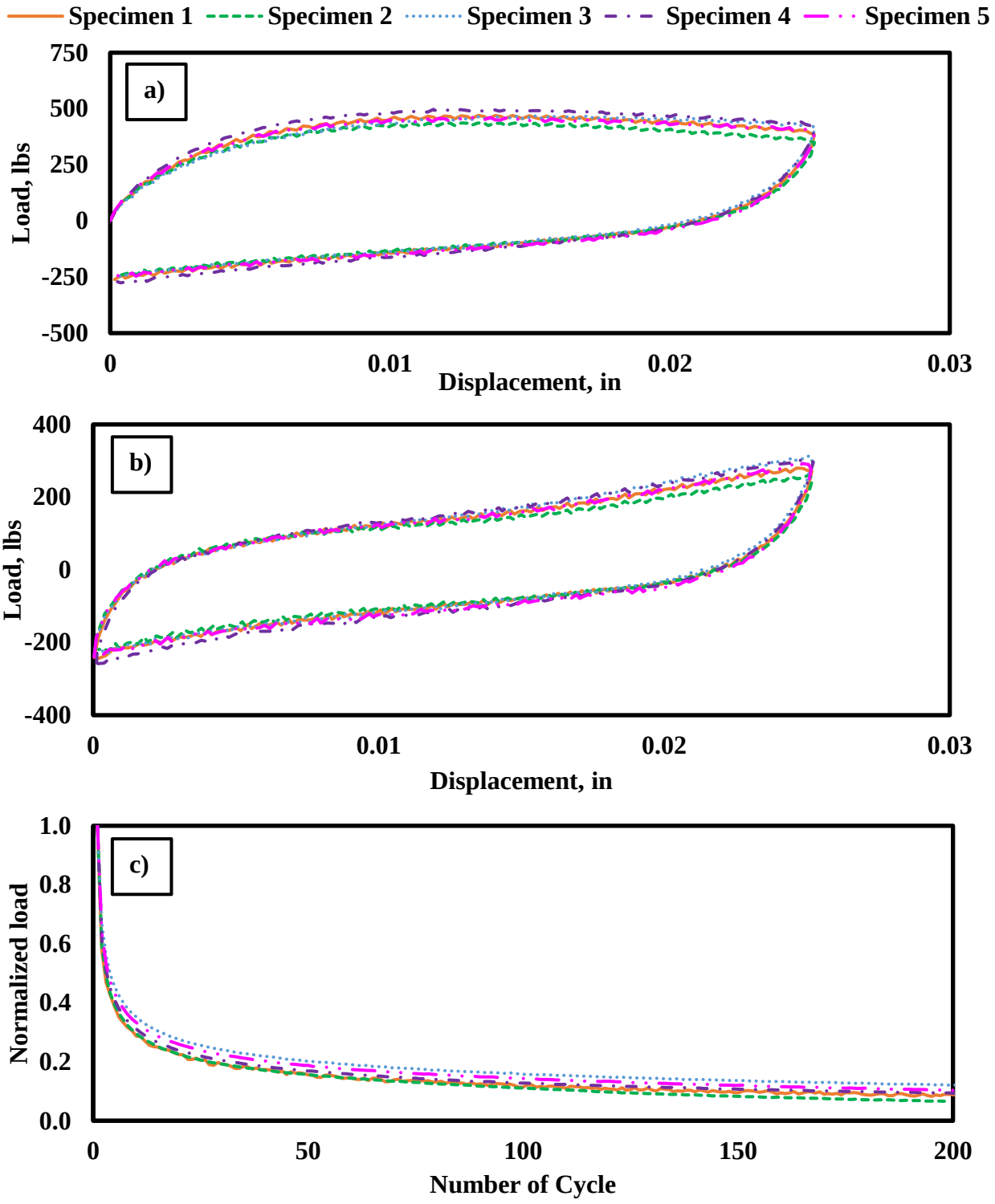

Figure B1: Results for Type-C Mix: a) First Cycle Hysteresis Loop, b) Second Cycle Hysteresis Loop, and c) Normalized Load Reduction

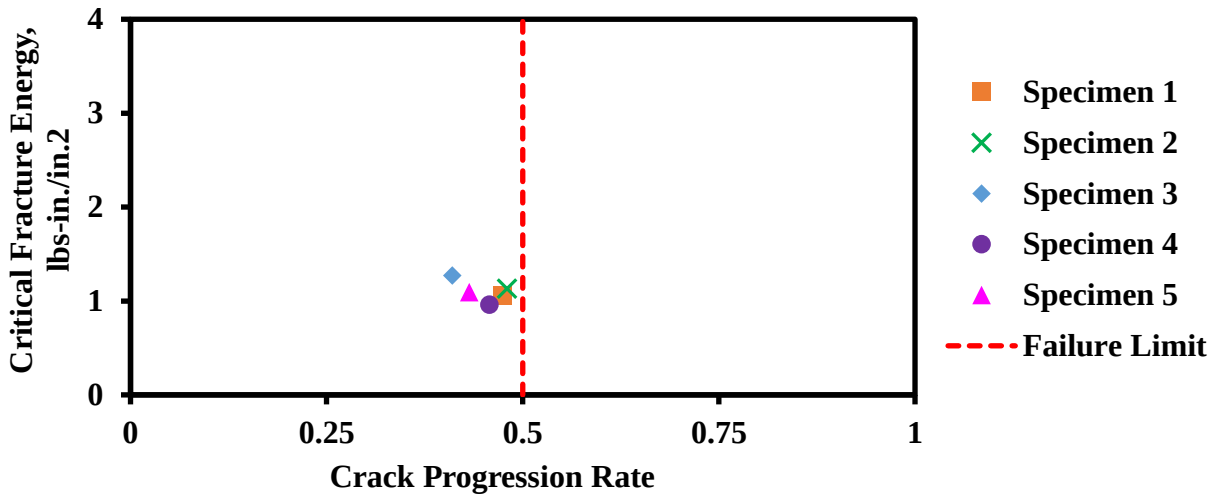

Figure B2: Performance of Type-C on Design Interaction Plot

Table B1: Summary of OT Results for Type-C Mix

Specimen	Air Voids, %	Max Load, lbs	Work of Fracture, in-lbs	Critical Fracture Energy, in.-lbs/in.^{2}	Crack Progression Rate	R^2	Number of Cycles to Failure
Specimen 1	7.6	470	4.8	1.1	0.47	1.00	312
Specimen 2	7.9	439	5.1	1.1	0.48	1.00	198
Specimen 3	7.4	469	5.7	1.3	0.41	1.00	483
Specimen 4	7.6	497	4.3	1.0	0.46	1.00	370
Specimen 5	7.2	461	4.9	1.1	0.43	1.00	389
Average	7.5	467	5.0	1.1	0.45	1.00	350
Std Dev	0.2	19	0.5	0.1	0.03	0.00	94
COV	**3%**	**4%**	**9%**	**9%**	**6%**	**NA**	**27%**

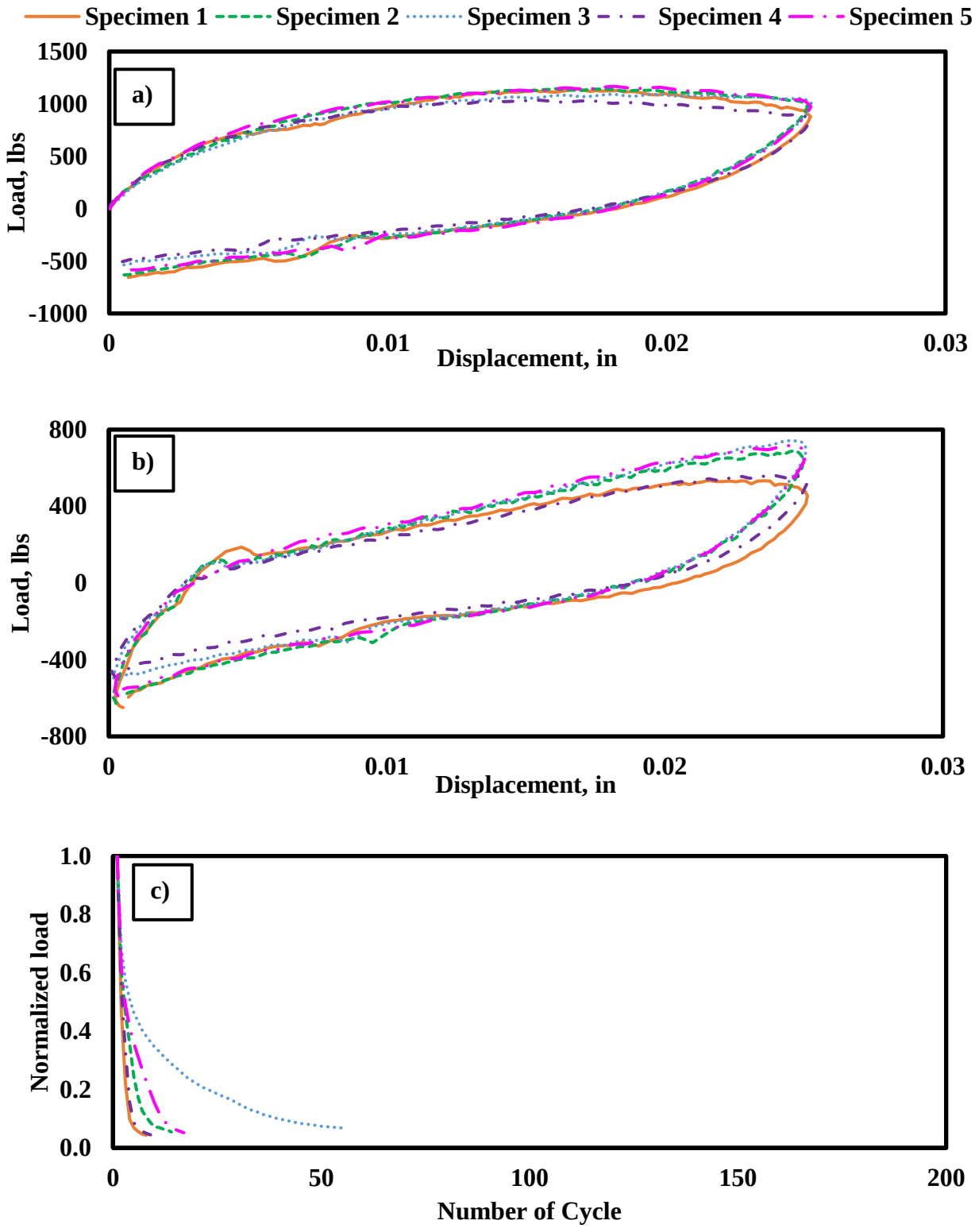

Figure B3: Results for Type-D Mix: a) First Cycle Hysteresis Loop, b) Second Cycle Hysteresis Loop, and c) Normalized Load Reduction

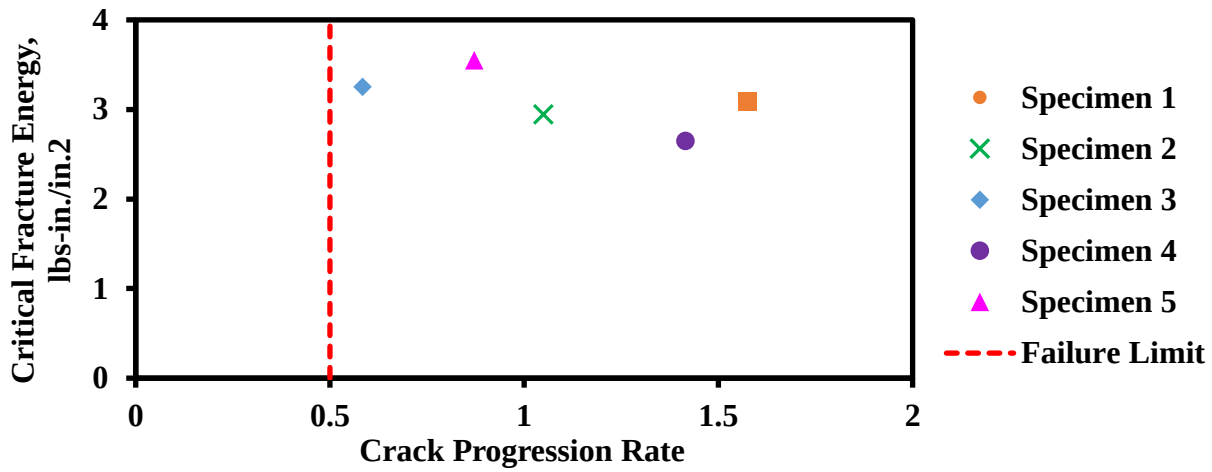

Figure B4: Performance of Type-D on Design Interaction Plot

Table B2: Summary of OT Results for Type-D Mix

Specimen	Air Voids, %	Max Load, lbs	Work of Fracture, in-lbs	Critical Fracture Energy, in.-lbs/in.^{2}	Crack Progression Rate	R^2	Number of Cycles to Failure
Specimen 1	7.6	1141	13.9	3.1	1.58	0.99	8
Specimen 2	7.9	1145	13.2	2.9	1.05	0.99	14
Specimen 3	7.4	1091	14.6	3.3	0.58	0.99	55
Specimen 4	7.6	1036	11.9	2.6	1.42	0.99	9
Specimen 5	7.2	1168	16.0	3.5	0.87	0.97	17
Average	7.5	1116	13.9	3.1	1.10	0.99	21
Std Dev	0.2	47	1.4	0.3	0.36	0.01	18
COV	**3%**	**4%**	**10%**	**10%**	**33%**	**1%**	**85%**

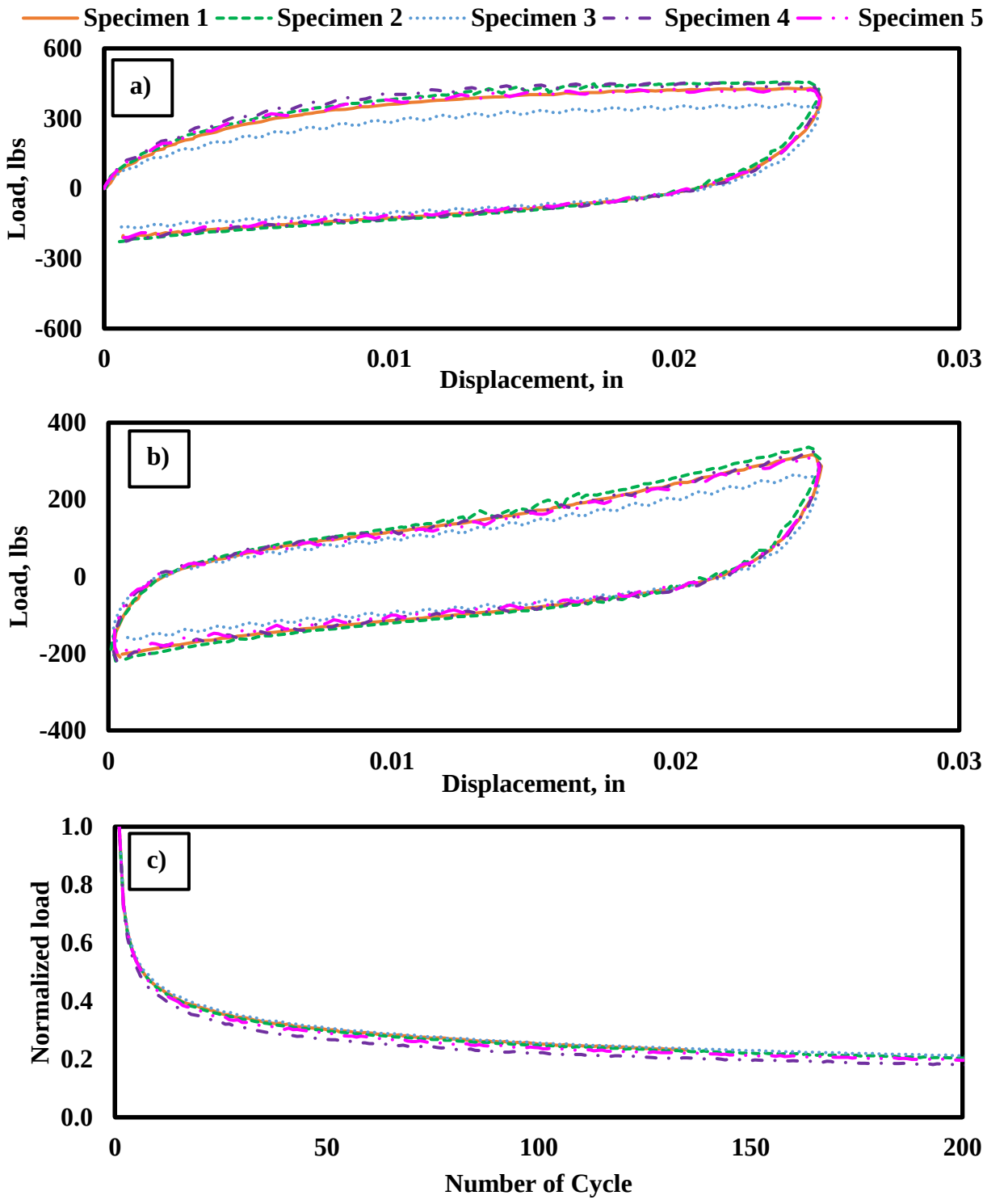

Figure B5: Results for SMA-D Mix: a) First Cycle Hysteresis Loop, b) Second Cycle Hysteresis Loop, and c) Normalized Load Reduction

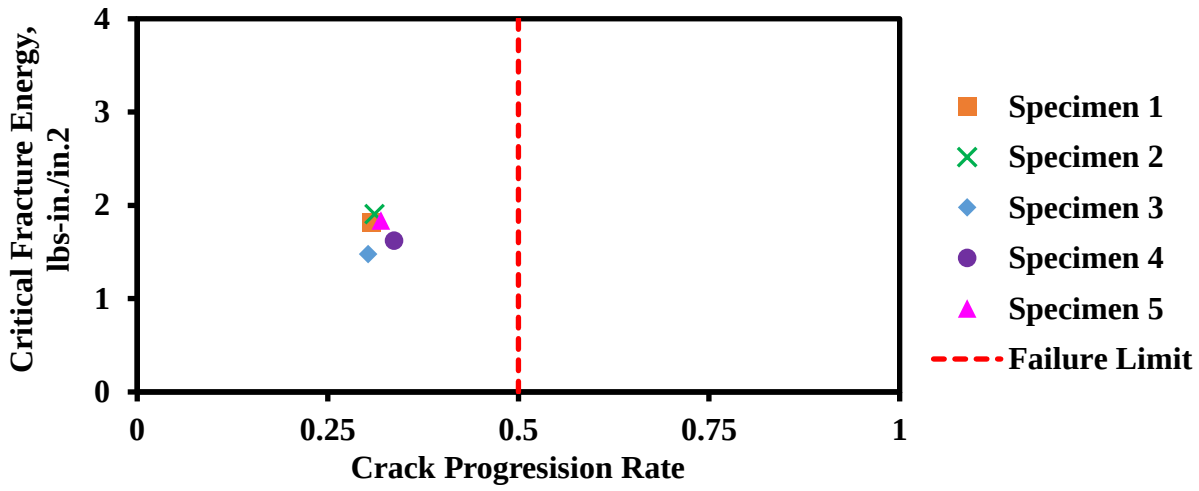

Figure B6: Performance of SMA-D on Design Interaction Plot

Table B3: Summary of OT Results for SMA-D Mix

Specimen	Air Voids, %	Max Load, lbs	Work of Fracture, in-lbs	Critical Fracture Energy, in.-lbs/in.^{2}	Crack Progression Rate	R^2	Number of Cycles to Failure
Specimen 1	6.9	429	8.2	1.8	0.31	1.00	1000
Specimen 2	7.7	457	8.6	1.9	0.31	1.00	1000
Specimen 3	6.6	362	6.7	1.5	0.30	1.00	1000
Specimen 4	6.4	452	7.3	1.6	0.34	1.00	1000
Specimen 5	6.2	428	8.3	1.8	0.32	1.00	1000
Average	6.8	426	7.8	1.7	0.32	1.00	1000
Std Dev	0.5	34	0.7	0.2	0.01	0.00	0
COV	**8%**	**8%**	**9%**	**9%**	**4%**	**NA**	**NA**

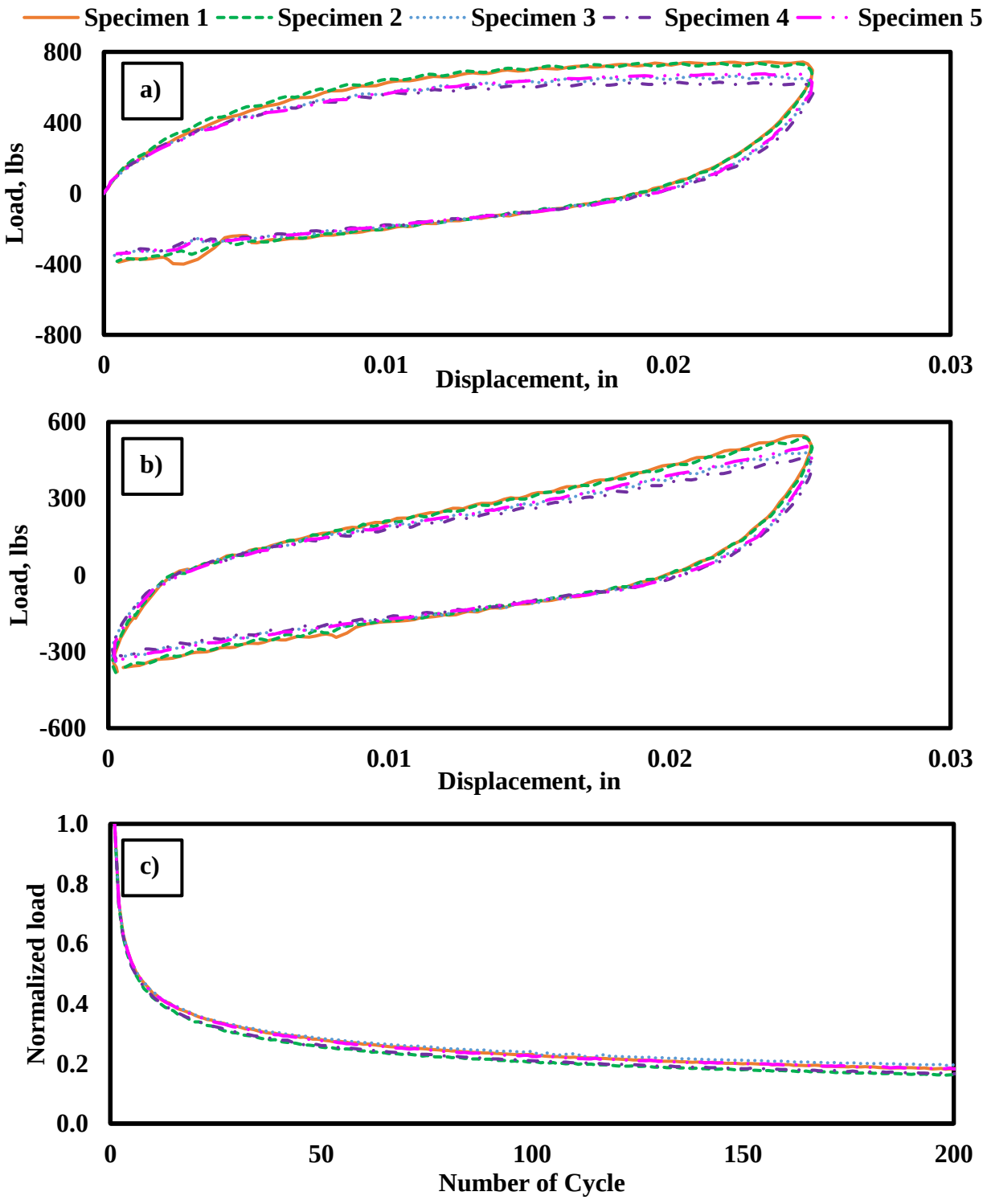

Figure B7: Results for TOM Mix: a) First Cycle Hysteresis Loop, b) Second Cycle Hysteresis Loop, and c) Normalized Load Reduction

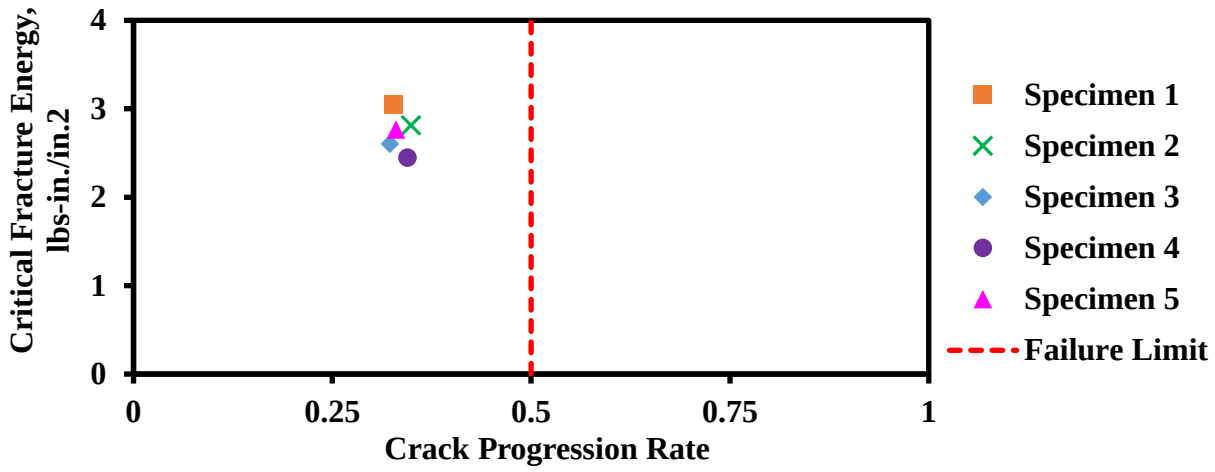

Figure B8: Performance of TOM on Design Interaction Plot

Table B4: Summary of OT Results for TOM Mix

Specimen	Air Voids, %	Max Load, lbs	Work of Fracture, in-lbs	Critical Fracture Energy, in.-lbs/in.^{2}	Crack Progression Rate	R^2	Number of Cycles to Failure
Specimen 1	7.6	742	13.7	3.1	0.33	1.00	1000
Specimen 2	7.9	737	12.7	2.8	0.35	1.00	1000
Specimen 3	7.4	663	11.7	2.6	0.32	1.00	1000
Specimen 4	7.6	629	11.0	2.4	0.34	1.00	1000
Specimen 5	7.2	676	12.5	2.8	0.33	1.00	1000
Average	7.5	689	12.3	2.7	0.33	1.00	1000
Std Dev	0.2	44	0.9	0.2	0.01	0.00	0
COV	**3%**	**6%**	**7%**	**7%**	**3%**	**NA**	**NA**

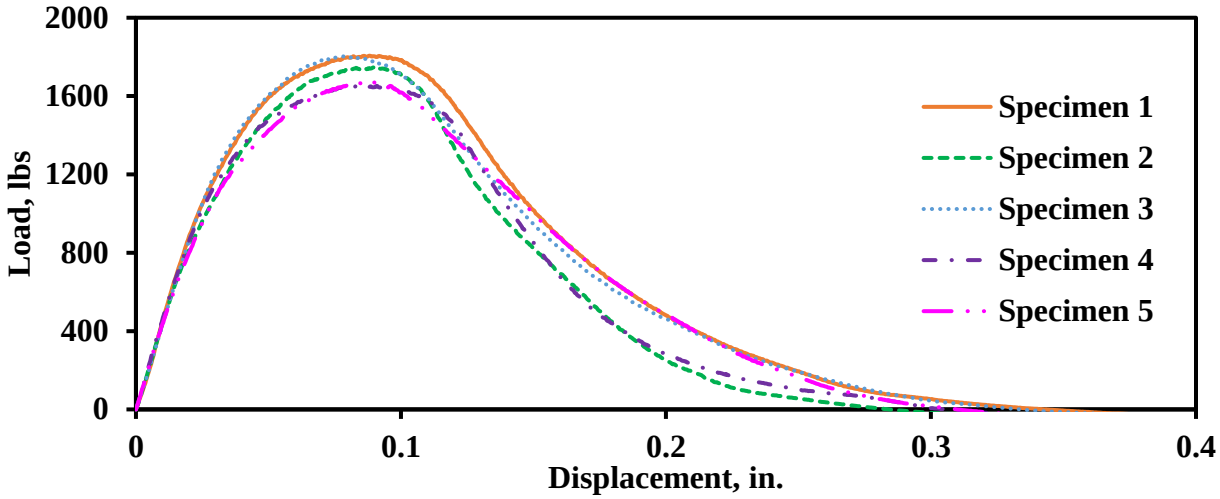

Figure B9: IDT Load-displacement Response Curves for Type-C Mix

Table B5: Summary of IDT Results for Type-C Mix

Specimen	Air Voids, %	Maximum Load, lbs	Tensile Modulus, psi	Tensile Strength, psi	Strain at Peak Load, %
Specimen 1	6.5	1806	14540	143	2.1
Specimen 2	6.8	1746	13947	138	2.1
Specimen 3	6.9	1803	14018	142	1.8
Specimen 4	7.0	1655	14190	130	2.1
Specimen 5	6.6	1672	13084	132	2.0
Average	6.8	1736	13956	137	2.0
Std Dev	0.2	71	539	6	0.1
COV	**3%**	**4%**	**4%**	**4%**	**5%**

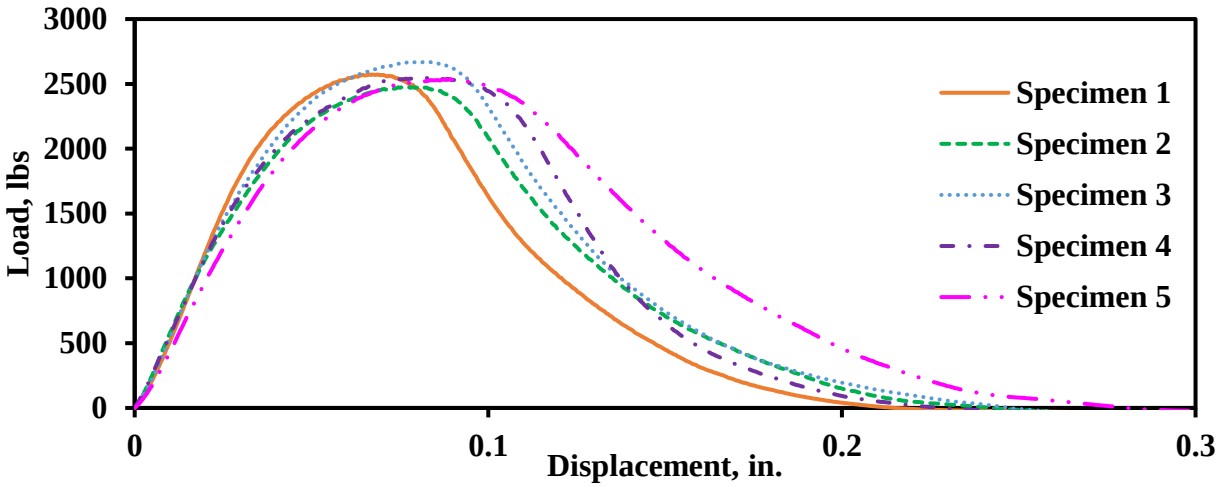

Figure B10: IDT Load-displacement Response Curves for Type-D Mix

Table B6: Summary of IDT Results for Type-D Mix

Specimen	Air Voids, %	Maximum Load, lbs	Tensile Modulus, psi	Tensile Strength, psi	Strain at Peak Load, %
Specimen 1	6.5	2572	20716	204	1.5
Specimen 2	7.3	2476	18633	196	1.8
Specimen 3	6.0	2670	19505	211	1.9
Specimen 4	6.7	2548	18850	202	2.0
Specimen 5	6.5	2535	16251	201	2.1
Average	6.6	2560	18791	203	1.9
Std Dev	0.5	71	1635	6	0.2
COV	**7%**	**3%**	**9%**	**3%**	**12%**

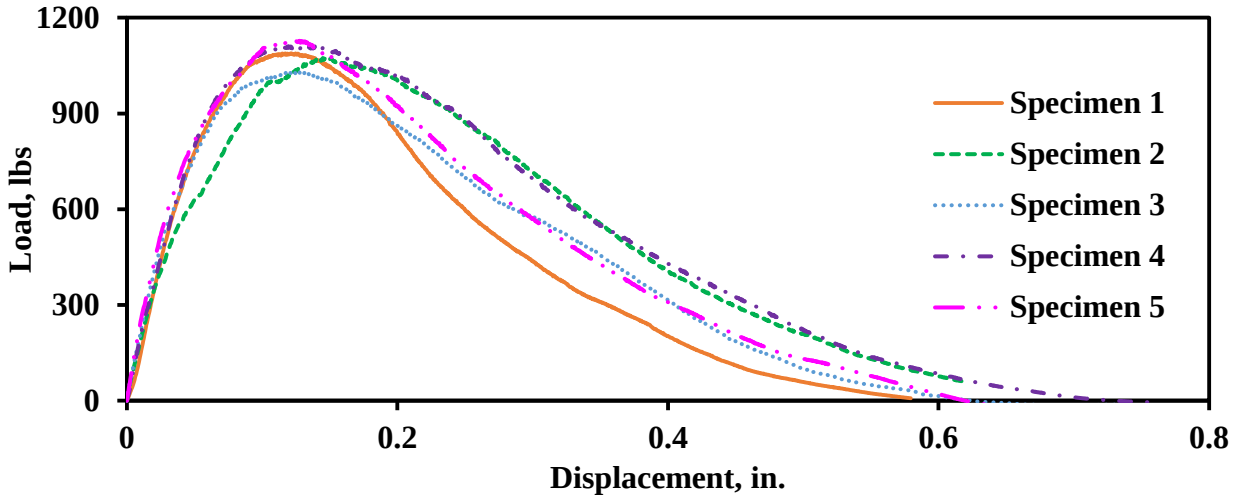

Figure B11: IDT Load-displacement Response Curves for SMA-D Mix

Table B7: Summary of IDT Results for SMA-D Mix

Specimen	Air Voids, %	Maximum Load, lbs	Tensile Modulus, psi	Tensile Strength, psi	Strain at Peak Load, %
Specimen 1	7.5	1088	5963	86	2.9
Specimen 2	7.0	1075	4810	85	3.6
Specimen 3	7.2	1031	6044	81	3.0
Specimen 4	7.2	1110	5361	88	3.0
Specimen 5	6.8	1128	6074	89	3.0
Average	7.1	1087	5651	86	3.1
Std Dev	0.3	37	553	3	0.3
COV	**4%**	**3%**	**10%**	**4%**	**10%**

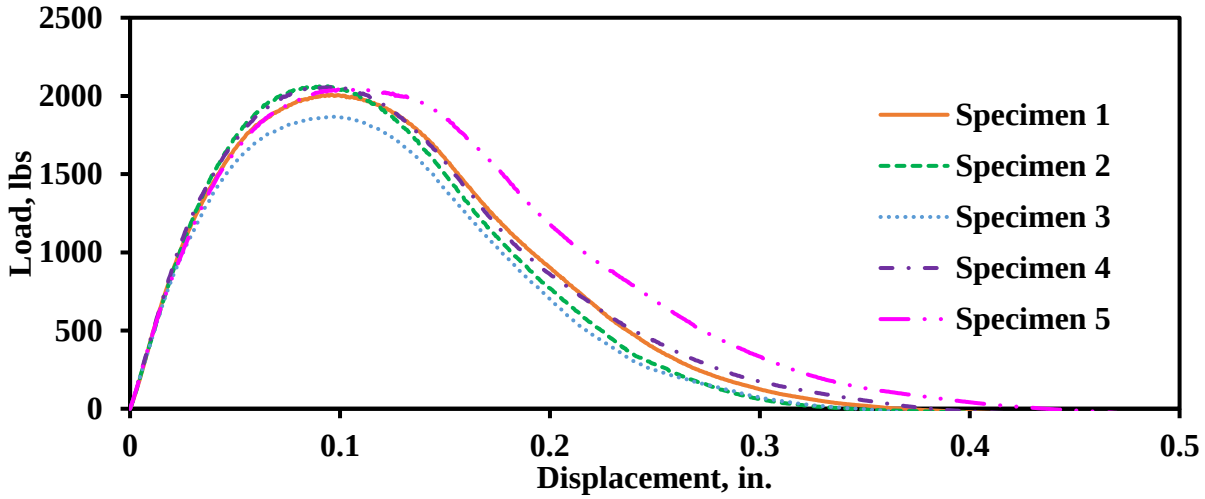

Figure B12: IDT Load-displacement Response Curves for TOM Mix

Table B8: Summary of IDT Results for TOM Mix

Specimen	Air Voids, %	Maximum Load, lbs	Tensile Modulus, psi	Tensile Strength, psi	Strain at Peak Load, %
Specimen 1	6.7	2007	14339	159	2.3
Specimen 2	6.8	2061	13667	163	2.2
Specimen 3	7.0	1867	13479	148	2.2
Specimen 4	7.2	2056	14317	163	2.3
Specimen 5	7.1	2045	12977	162	2.5
Average	7.0	2007	13756	159	2.3
Std Dev	0.2	81	580	6	0.1
COV	**3%**	**4%**	**4%**	**4%**	**5%**

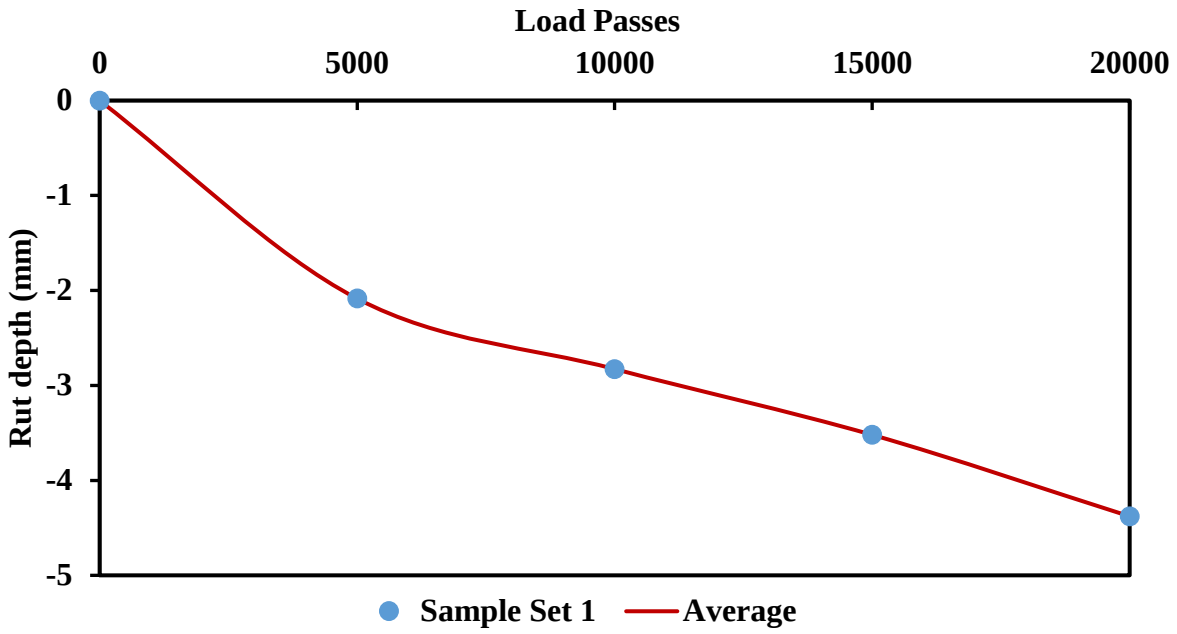

Figure B13: Rut Depth of One Sample for Type-C Mix

Table B9: Summary of HWTD Results for Type-C Mix

Specimen	Air Voids, %	Rut Depth, mm after			
		5000 Passes	10000 Passes	15000 Passes	20000 Passes
Specimen 1	7.8	2.1	2.8	3.5	4.4
Specimen 2	7.6				
Average	7.7				
Std Dev	0.1				
COV	**2%**				

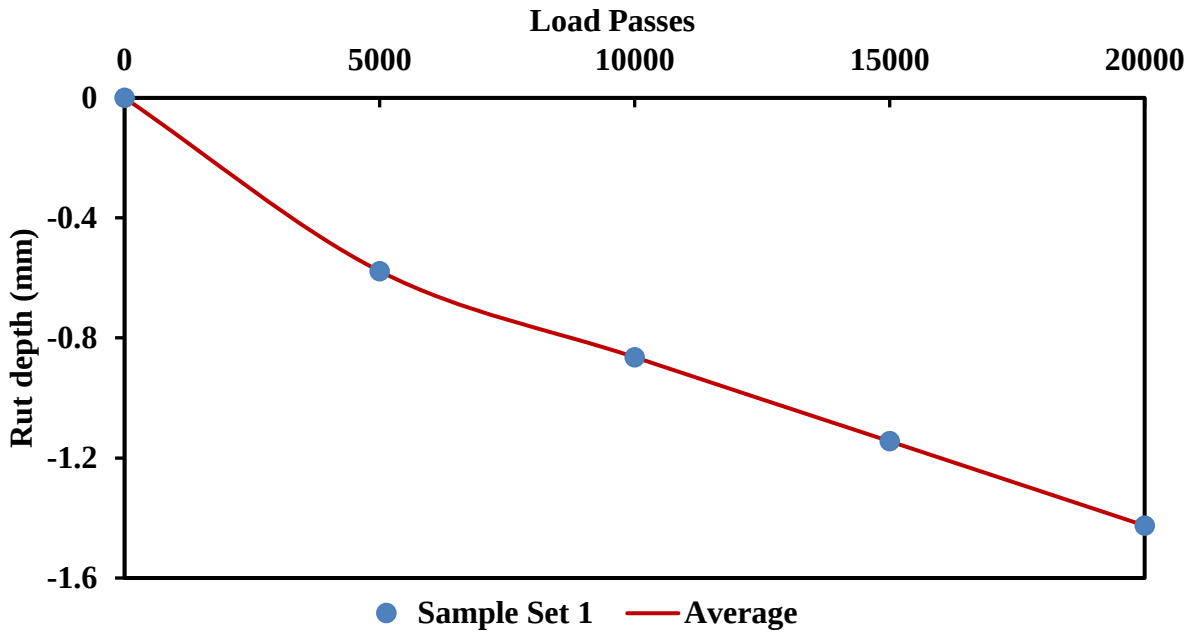

Figure B14: Rut Depth of One Sample for Type-D Mix

Table B10: Summary of HWTD Results for Type-D Mix

Specimen	Air Voids, %	Rut Depth, mm after			
		5000 Passes	10000 Passes	15000 Passes	20000 Passes
Specimen 1	7.4	0.6	0.9	1.1	1.4
Specimen 2	7.4				
Average	7.4				
Std Dev	0.0				
COV	**NA**				

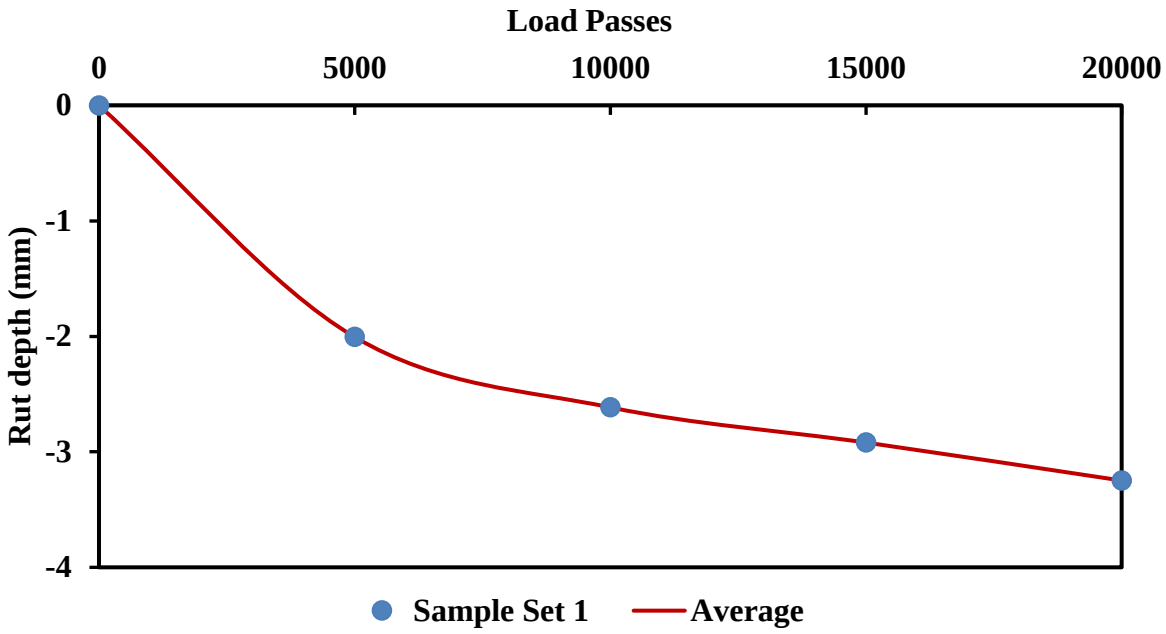

Figure B15: Rut Depth of One Sample for SMA-D Mix

Table B11: Summary of HWTD Results for SMA-D Mix

Specimen	Air Voids, %	Rut Depth, mm after			
		5000 Passes	10000 Passes	15000 Passes	20000 Passes
Specimen 1	7	2.0	2.6	2.9	3.2
Specimen 2	7.2				
Average	7.1				
Std Dev	0.1				
COV	**2%**				

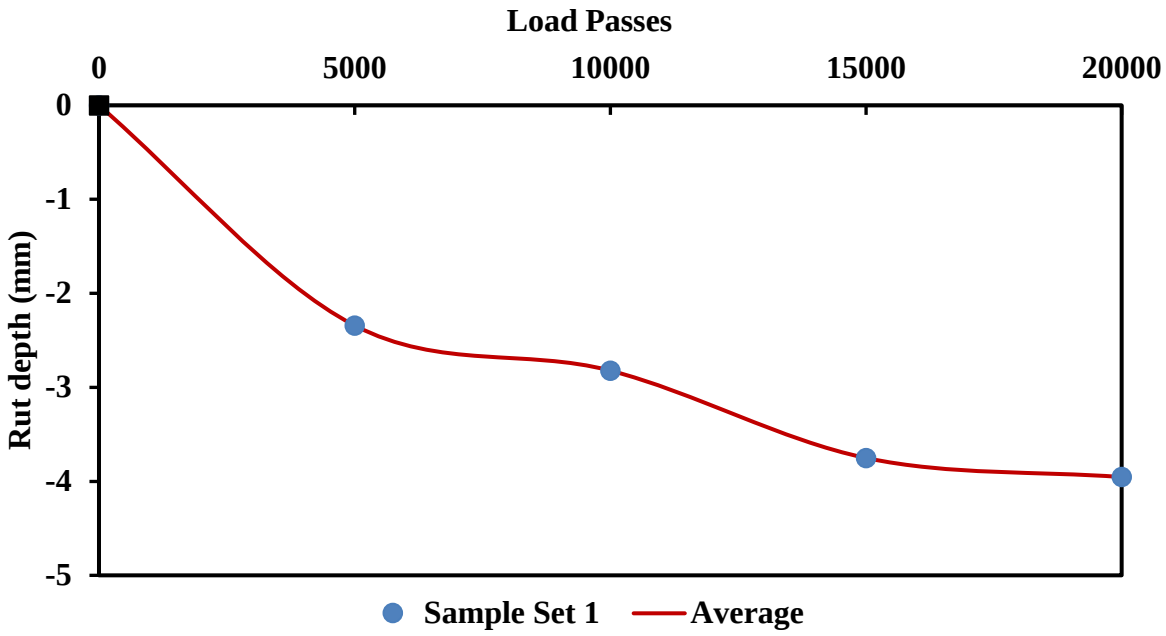

Figure B16: Rut Depth of One Sample for TOM Mix

Table B12: Summary of HWTD Results for TOM Mix

Specimen	Air Voids, %	Rut Depth, mm after			
		5000 Passes	10000 Passes	15000 Passes	20000 Passes
Specimen 1	7.4	2.0	2.6	2.9	3.2
Specimen 2	7.7				
Average	7.55				
Std Dev	0.2				
COV	**3%**				

Vita

Isaac Aguilar was born in Tyler, Texas and graduated from Robert E. Lee High School in 2011. He attended The University of Texas at Tyler to pursue a Bachelors in Civil Engineering and received his degree in the spring of 2015. As an undergraduate he had the opportunity to work as an intern twice with the Texas Department of Transportation (TxDOT) which started his interest in transportation engineering. As an undergraduate student he also worked as a tutor and soccer coach during the school year. In the summer prior to his senior year, he was accepted to participate in the Louis Stokes Alliance for Minority Participation (LSAMP) summer research program at The University of Texas at El Paso (UTEP). There he worked at the Center for Transportation for Infrastructure Systems (CTIS) and decided to return to enroll in the master's program at UTEP under the guidance of Dr. Soheil Nazarian.

At CTIS, Mr. Aguilar worked with other fellow graduate student researchers on different research projects in pavement design. As a graduate student, he was selected as a Dwight D. Eisenhower Transportation Fellow and a HENAAC Scholar. He was also a member in different student organizations such as the American Society of Civil Engineering (ASCE) and Chi Epsilon National Civil Engineering Honor Society. He completed a Master's Degree in Civil Engineering in the spring of 2017.

Contact Information: ijaguilar2@miners.utep.edu

This thesis was typed by Isaac Jaime Aguilar**)**